NREL
NATIONAL RENEWABLE ENERGY LABORATORY

Controller Field Tests on the NREL CART2 Turbine

E. Bossanyi
Garrad Hassan & Partners Ltd.

A. Wright and P. Fleming
National Renewable Energy Laboratory

NREL is a national laboratory of the U.S. Department of Energy, Office of Energy Efficiency & Renewable Energy, operated by the Alliance for Sustainable Energy, LLC.

Technical Report
NREL/TP-5000-49085
December 2010

Contract No. DE-AC36-08GO28308

NREL
NATIONAL RENEWABLE ENERGY LABORATORY

Controller Field Tests on the NREL CART2 Turbine

E. Bossanyi
Garrad Hassan & Partners Ltd.

A. Wright and P. Fleming
National Renewable Energy Laboratory

Prepared under Task No. WE10.3131

National Renewable Energy Laboratory
1617 Cole Boulevard
Golden, Colorado 80401
303-275-3000 • www.nrel.gov

Technical Report
NREL/TP-5000-49085
December 2010

Contract No. DE-AC36-08GO28308

NOTICE

Available electronically at http://www.osti.gov/bridge

Available for a processing fee to U.S. Department of Energy
and its contractors, in paper, from:

U.S. Department of Energy
Office of Scientific and Technical Information

P.O. Box 62
Oak Ridge, TN 37831-0062
phone: 865.576.8401
fax: 865.576.5728
email: mailto:reports@adonis.osti.gov

Available for sale to the public, in paper, from:

U.S. Department of Commerce
National Technical Information Service
5285 Port Royal Road
Springfield, VA 22161
phone: 800.553.6847
fax: 703.605.6900
email: orders@ntis.fedworld.gov
online ordering: http://www.ntis.gov/help/ordermethods.aspx

Cover Photos: (left to right) PIX 16416, PIX 17423, PIX 16560, PIX 17613, PIX 17436, PIX 17721

Printed on paper containing at least 50% wastepaper, including 10% post consumer waste.

Abstract

This document presents the results of the field tests carried out on the CART2 turbine at NREL to validate control algorithms for individual pitch control and active tower damping designed for this turbine by Garrad Hassan & Partners Ltd as part of the European research project ‘UPWIND’.

Table of Contents

Figures

Tables

Introduction

An important task of the UPWIND control systems work package is to use field tests to demonstrate that the very significant load reductions predicted with individual pitch control (IPC) can really be achieved in practice. So far, the only published results have come from simulation models [1], so field test results are vital for increasing the confidence of turbine designers to use IPC in their new designs to improve cost-effectiveness.

As well as reducing asymmetrical out of plane loading on three-bladed machines, IPC can similarly be used on two-bladed machines to replace a mechanical teeter hinge [2]. Two-bladed turbines are still in contention for use offshore, since some of the main environmental impact objections are less relevant in that environment, i.e. aerodynamic noise due to high tip speed, and visual appearance. Although the hub fatigue loads will still be higher than with a completely free teeter hinge, some form of teeter restraint is often required in practice. This reintroduces some loading, and the possibility of extreme load damage due to teeter end-stop impacts.
In any case, the advanced control principles to be tested (both IPC and tower damping), are actually identical, irrespective of the number of blades. The IPC control action is calculated in the non-rotating frame in two orthogonal axes, and this is equally valid for any number of blades.

Field tests were originally intended for a commercial European turbine, but commercial considerations prevented this testing. Therefore, a new program was conceived in 2008, making use of two research turbines at the NREL test site in Colorado, USA. Both Controls Advanced Research Turbines (CART's) are 42m in diameter and rated at 660 kW. Because the CART2 is two bladed and the CART3 is three-bladed, they provided an excellent opportunity to test IPC in both cases. Although these turbines may be a bit small and commercially unrepresentative, they are quite adequate for the required proof of principle, and have the advantage of being very accessible and free of commercial problems that might prevent publication of results. Some of the field test results have been published in [3],[4] and a full report is available in [5].

At the same time, they offer the opportunity to further confirm the efficacy of fore-aft tower damping (FATD) by means of collective pitch control. Although this has previously been demonstrated in the field [6], the present tests provided an ideal opportunity to provide further experimental verification of this technique.
This document presents the results of the field tests carried out on the two-bladed CART2 turbine at NREL, and demonstrates conclusively that both IPC and FATD can reduce fatigue loading as anticipated.

The CART2 turbine

The CART2 turbine is 42m in diameter, with a rated output of 660 kW at 41.7 rpm rotor speed. For these tests the rated power was set at 570 kW which is reached at about 12.7 m/s wind speed. The machine is two-bladed with a teetered hub. The aim of the IPC is to avoid the need for a teetered hub, but the turbine has a teeter brake, which was applied during the tests to lock the teeter hinge.

The CART-2 is fitted with conventional strain gauges, but these are very stable, robust and well calibrated. This is partly because of the mounting position, made possible by the spindle bearings used for pitching, which also results in very low pitch bearing friction and very fast actuator response, which is very suitable for IPC. This is excellent for proving the control principles, even if it does not allow experience to be built up with the use of fiber-optic load sensors (which are more likely to be chosen for commercial applications) or the effect on more conventional pitch bearings or actuation systems.

A *Bladed* model of the CART-2 turbine was built from information supplied by NREL [7]. Details are provided in Appendix A.

Linearized models were derived from this at a number of operating points, and used as the starting point for control tuning. A Campbell diagram showing the coupled system modes is shown in Figure 1. The lowest key frequencies are listed in Table 1. Some of the frequencies do not match exactly with those measured on the real turbine; however, as the advanced control techniques being tested here are expected to be reasonably robust, no further effort was made to match the model exactly to the turbine. The experimental results certainly have helped to confirm this robustness.

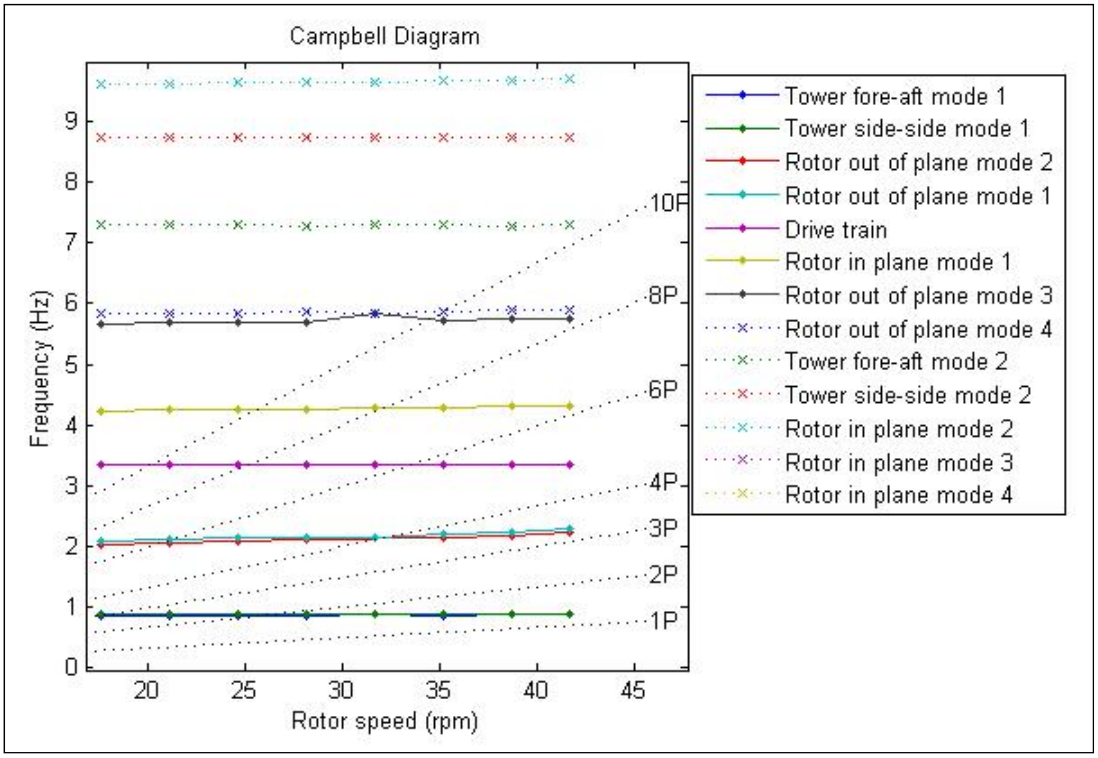

Figure 1. CART2 Campbell diagram

Table 1. Lowest key frequencies, as modeled

Rated rotational frequency (1P)	0.695	Hz
Blade passing frequency (2P)	1.39	Hz
First fore-aft tower mode	0.88	Hz
First rotor out of plane mode	2.22	Hz
Drive train torsion	3.36	Hz
First rotor in-plane mode	4.31	Hz

Controller design

The power production control algorithm to be tested on the CART2 is based on up-to-date principles regularly used by Garrad Hassan (GH) for commercial controller design work [1],[8]. The application of these techniques to the UPWIND 5 MW reference turbine is documented in [9],[10]. The application of these techniques to the CART2 is similar and, therefore, not elaborated here in detail.
The controller includes the following features:

- Optimal power production, maintaining peak Cp over the entire nominal operating speed range
- Speed regulation by interacting PI-based torque and collective pitch control loops
- Drivetrain damping filter in torque controller
- Damping of fore-aft tower vibration by collective pitch control
- PI-based 1P individual pitch control to reduce rotating and non-rotating loads

The tuning of the control loops has been carried out using classical design techniques. Although the controller as a whole has several measured input signals and several output demands, it can easily be divided into a series of largely decoupled single-input, single-output loops for which classical methods are well suited. For those loops which are not fully decoupled, for example the collective pitch control loops for rotor speed and tower vibration, a good coupled solution can be reached after only a very small number of iterations with each loop in turn. In many ways, this is more practical than using multivariable methods.

Of particular relevance to this work, the IPC control is decoupled into two orthogonal PI control loops, tuned identically, thus ignoring the azimuthal asymmetry in the turbine dynamics due to the tower. The tower damper was tuned in parallel with the pitch PI controller using an iterative approach, but a single iteration was sufficient.
The main controller parameters are listed in Table 2. The drivetrain damper is not included, for reasons explained below.

For the field testing, the IPC and FATD action can be switched on and off during operation without affecting speed regulation. By comparing test data with and without the advanced features, the load reduction can be quantified across a variety of wind conditions.

Table 2: Controller parameters

Parameter	Value	Units
Minimum generator speed	1295	rpm
Optimal mode quadratic speed-torque gain	0.081997	Nms²/rad²
Rated generator speed	1800	rpm
Generator torque set point	3524.36	Nm
Fine pitch angle	-1	deg
Dead-band	0.1	deg
Maximum negative pitch rate	-18	deg/s
Maximum positive pitch rate	18	deg/s
Pitch position error adjustment gain	1	s^{-1}
Nominal pitch controller proportional gain	0.02127	s
Nominal pitch controller integral gain	0.01820	-
Gain schedule	Inverse linear on pitch angle	-
Gain divisor below 7º	1	-
Gain divisor above 49º	7.8	-
Power-pitch proportional gain	1.e-6	rad/W
Power-pitch integral gain	1.e-6	rad/Ws
Pitch controller notch filter 1	8.7178, 0, 8.20266, 0.06072	*Note 1*
Pitch controller notch filter 2	8.7178, 0, 9.26528, 0.06072	*Note 1*
Pitch controller notch filter 3	21.031, 0.3507, 17.66, 0.5755	*Note 1*
Pitch controller notch filter 4	20.5, 0.0077, 20.5, 0.0971	*Note 1*
Tower damping gain	0.01614	rad/m
Tower damping filter	2.8, 0.8878, 4.713, 0.437	*Note 1*
Accelerometer high-pass filter frequency	0.6283	rad/s
Accelerometer high-pass filter damping	0.7071	rad/s
IPC maximum amplitude (*Note 2*)	5	deg
IPC proportional gain	1.1416e-7	deg/Nm
IPC integral gain	5.2514e-7	deg/Nms
IPC notch filter	8.73372, 0, 8.73372, 1	*Note 1*
IPC low pass filter frequency	20	rad/s
IPC low pass filter damping factor	1	-
IPC azimuthal compensation time shift	0.01	s
Azimuthal dead-band	0.001	rad
Torque controller proportional gain	264	Nms/rad
Torque controller integral gain	132	Nm/rad
Torque controller notch filter	25.131, 0, 5.02163, 0.919122	*Note 1*

Note 1: Numerator frequency (rad/s), numerator damping factor, denominator frequency (rad/s),

Note 2: Reduced to 2.9º during tests to avoid pitch actuator thermal stress

Field tests

The CART2 baseline controller at NREL is compiled from C and runs on a DOS computer. In early 2009, following simulation testing using Bladed [2], the new power production algorithm was embedded within the existing controller code. This already included the supervisory control, which hands over control to the new algorithm when a certain rotational speed is reached, but continues to monitor for faults and resumes control for shutdowns. Unfortunately, a gearbox failure occurred just before testing was due to begin, delaying the start of field testing until November 2009. There followed a winter wind season with unusually low winds, so that the first data was not obtained until early February 2010. The first results demonstrated good performance of the advanced load reduction features of the controller, as shown below. Testing continued, whenever sufficient wind was available, until mid-April 2010, allowing datasets to be collected over a good range of wind conditions.

Instrumentation

The sensor inputs to the control algorithm were:

- Rotor speed
- Rotor azimuth
- Generator speed
- Flapwise and edgewise blade root strain gauges (conventional type)
- Fore-aft nacelle acceleration
- Pitch angles

The following additional sensors were also used in evaluating the field test results:

- Wind speed and direction at hub height on nearby met mast
- Tower base bending strain gauges in two directions: E/W and N/S
- Nacelle yaw position
- Teeter angle
- Generator power

A number of internal controller variables were also logged, including the switching variable, which defines whether the IPC and FATD features are active.

Controller adjustments

The new control algorithm designed for CART2 included the following control features:

1. Drivetrain damper.
2. Speed regulation by torque (below rated).
3. Speed regulation by collective pitch (above rated).
4. Interaction between loops 2 and 3 around rated.
5. Fore-aft tower damping by collective pitch.
6. 1P individual pitch control using blade root strain gauges.

Features 5 and (more especially) 6 were the focus of the field tests. The performance of features 2, 3, and 4 was not quantified, but these were observed to work very well from the start, and required no adjustment. The design of the drivetrain damper (feature 1) depends on precise knowledge of the drivetrain dynamics and power converter control, for which the necessary level of detail was not available. The damper was designed to use generator speed as its input, but it was found that the filtered rotor speed was found to work better, and gave satisfactory performance. No attempt was made to analyze or optimize this feature since its problems are well understood and were not the focus of this exercise.

The advanced features 5 and 6 would normally be phased out in low winds, since the already low loading levels do not justify the additional pitch action required to reduce them further. For these tests however, these features were enabled at all wind speeds to maximize the amount of useful data obtained.

First results

All recorded datasets were 10 minutes in length. Headers were created to allow each dataset to be plotted and post-processed using Bladed.
Figure 2 plots four variables from dataset 02050340 measured on 4th February 2010 (at 8:40 p.m. Mountain Standard Time [MST]), just to illustrate the entirely satisfactory operation of the speed regulation below and above rated.

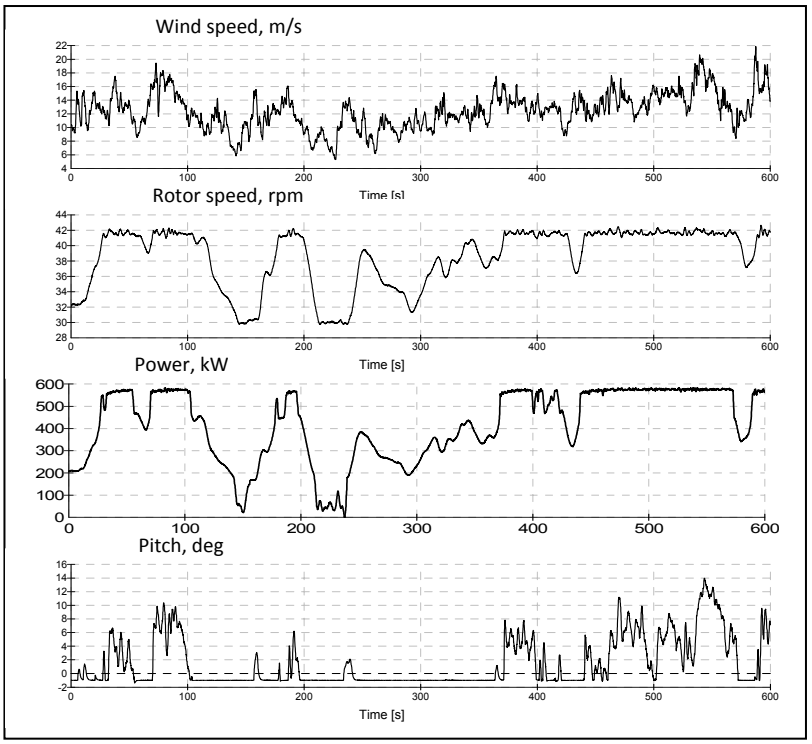

Figure 2. Speed regulation around rated

When the tower feedback feature was switched on, a problem was immediately apparent. The acceleration signal had a large mean offset (which is clearly not physical

if the turbine is staying in the same place). The integrator in the FATD algorithm was then causing the pitch angle to drift away, causing loss of power. If the pitch drifted to negative angles, the blades would stall and the IPC would work poorly, as predicted by simulations. The problem is illustrated in Figure 3 (part of dataset 01240204 from 3rd February 2010, measured at 7:04 p.m. MST).

This problem was very easily fixed by passing the acceleration signal through a 0.1 Hz high pass filter. This removed the offset with little effect on the phase of the remaining signal. After this change, both the IPC and FATD were found to work well, as the subsequent results illustrate.

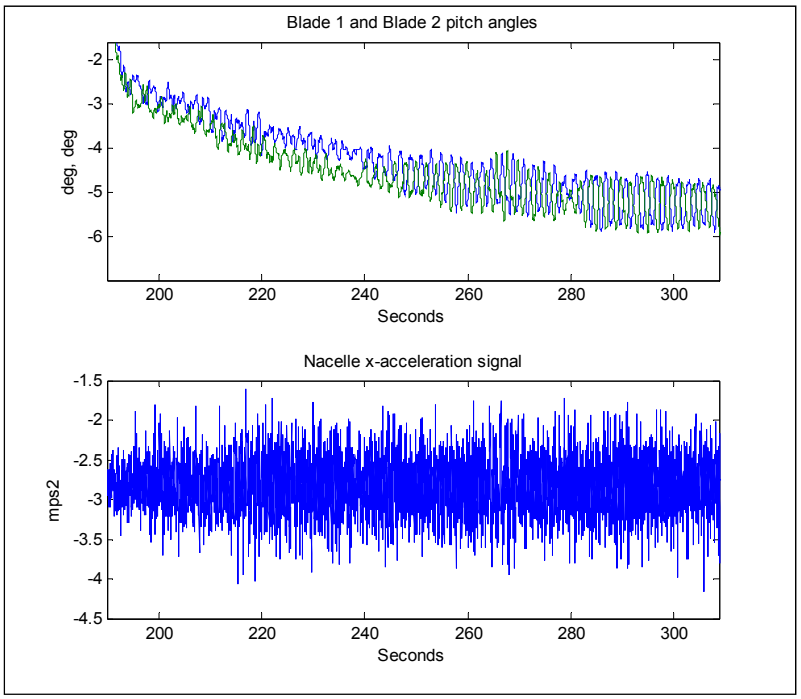

Figure 3. Effect of acceleration offset

Analysis of individual campaigns

First, some time series results are presented, comparing two datasets with similar wind conditions, both measured on 4th February 2010; dataset 02050253 with IPC and FATD switched 'OFF', and dataset 02050317 with both features switched 'ON' (Figure 4). Clearly the wind speed is not identical in the two cases, and is dropping off towards the end in case 'ON'. Fine pitch is reached (-1º) and the speed and power start to fall. The individual pitch action is clearly visible. The load reduction in the 'ON' case is not immediately obvious in the time histories. To assess this, Bladed post-processing was used to resolve the flapwise and edgewise bending moments, with pitch angle to give the out of plane moment, and the N/S and E/W tower base bending moments with yaw position to give the fore-aft moment (the yaw position signal was very noisy and first had to be cleaned up by removing spikes and filtering). Furthermore, the blade root My signals were combined to give the rotating hub My (ignoring the small additional moment due to differences in blade root Fx force). They were also transformed to stationary coordinates using the azimuth position, to give the hub fixed My and Mz

(ignoring any possible differences in blade Mz pitch moment). Spectra of these signals then immediately reveal the expected changes in loading.

Although the 'ON' case has a lower mean wind speed, it has significantly higher turbulence intensity, as shown in Table 3. Two more cases have, therefore, also been included in the subsequent analysis. These were selected to have similar wind speeds and turbulence intensities, but in this case slightly lower values in the 'ON' case. The characteristics of these datasets are also seen in Table 3. The table also includes an estimate of the wind shear, obtained as an approximate fit to the mean wind speeds measured at the four anemometer heights on the met mast: 3, 15, 36.6 and 58.2m.

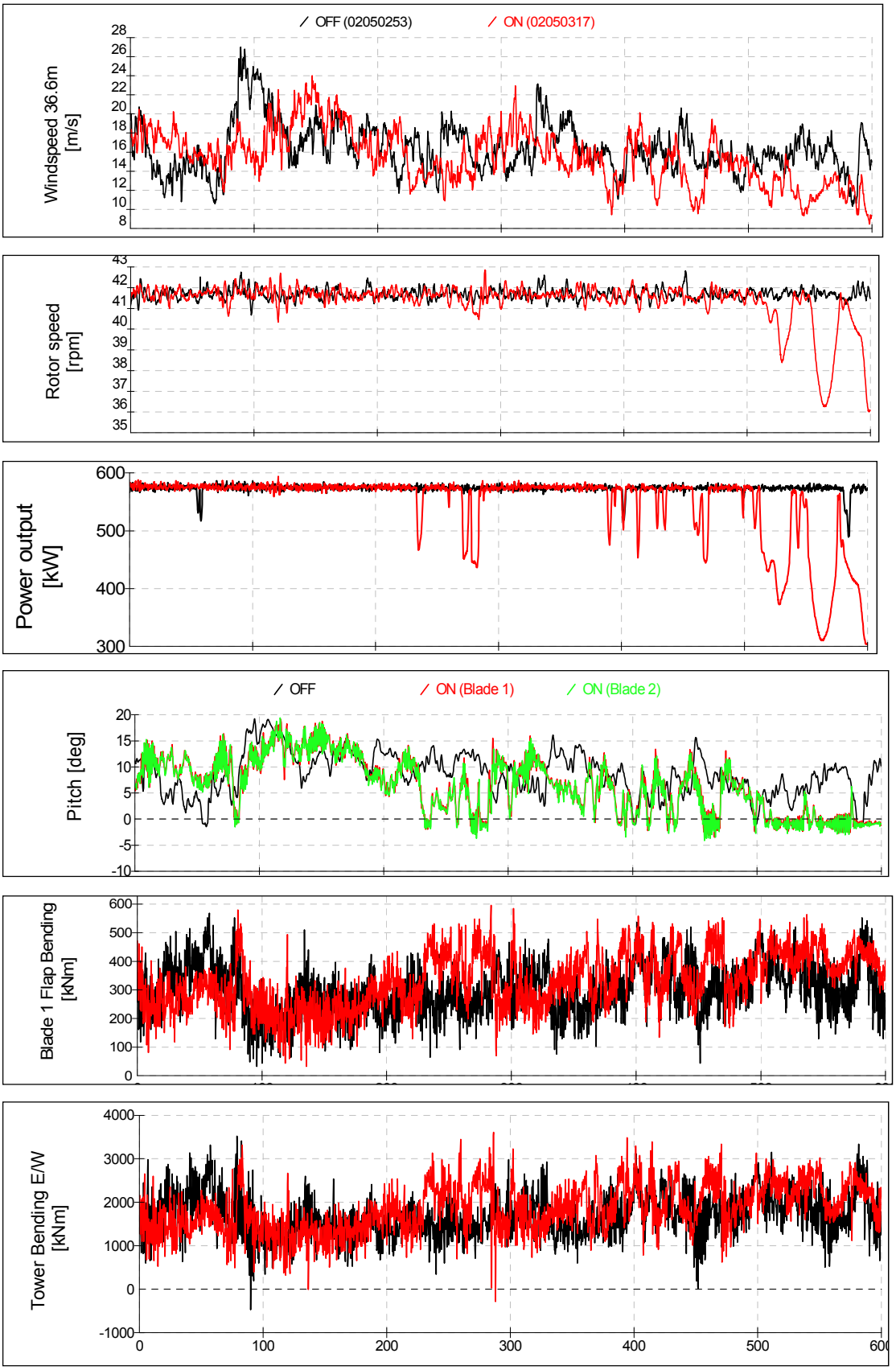

Figure 4. First results with and without IPC and FATD: 600s datasets near rated

Table 3. Sample datasets for comparison

Dataset	Mean wind direction (deg)	Mean wind speed (m/s)	Standard deviation (m/s)	Turbulence intensity (%)	Estimated shear exponent
02050253 (OFF) (7:53 p.m. MST)	276.698	16.3807	2.61317	15.95	.09
02050317 (ON) (8:17 p.m. MST)	284.246	15.481	2.85928	18.47	.14
02050340 (OFF) (8:40 p.m. MST)	289.563	12.4217	2.67643	21.55	.13
02020007 (ON) (5:07 p.m. MST)	277.872	12.0926	2.50302	20.70	.08

Looking first at the tower damping, Figure 5 shows the spectrum of tower base fore-aft bending moment for these four cases, with the thicker lines representing the two 'ON' cases. A clear reduction is seen on both 'ON' cases at the first tower frequency, around 0.9 Hz, confirming that the damping algorithm is working as intended. The low frequency levels are more variable, lower in one 'ON' case and higher in the other. This is simply caused by the range of the wind speed variations during the sample, not by the controller dynamics (more below rated dips occurred in the first 'ON' case). Since the maximum thrust occurs at rated, this gave rise to more periods of higher mean thrust in this case, as is clearly shown in Figure 4. For the 12 m/s cases, the 'OFF' case suffered from bigger wind speed dips down to 6 m/s, compared to 8 m/s for the 'ON' case.

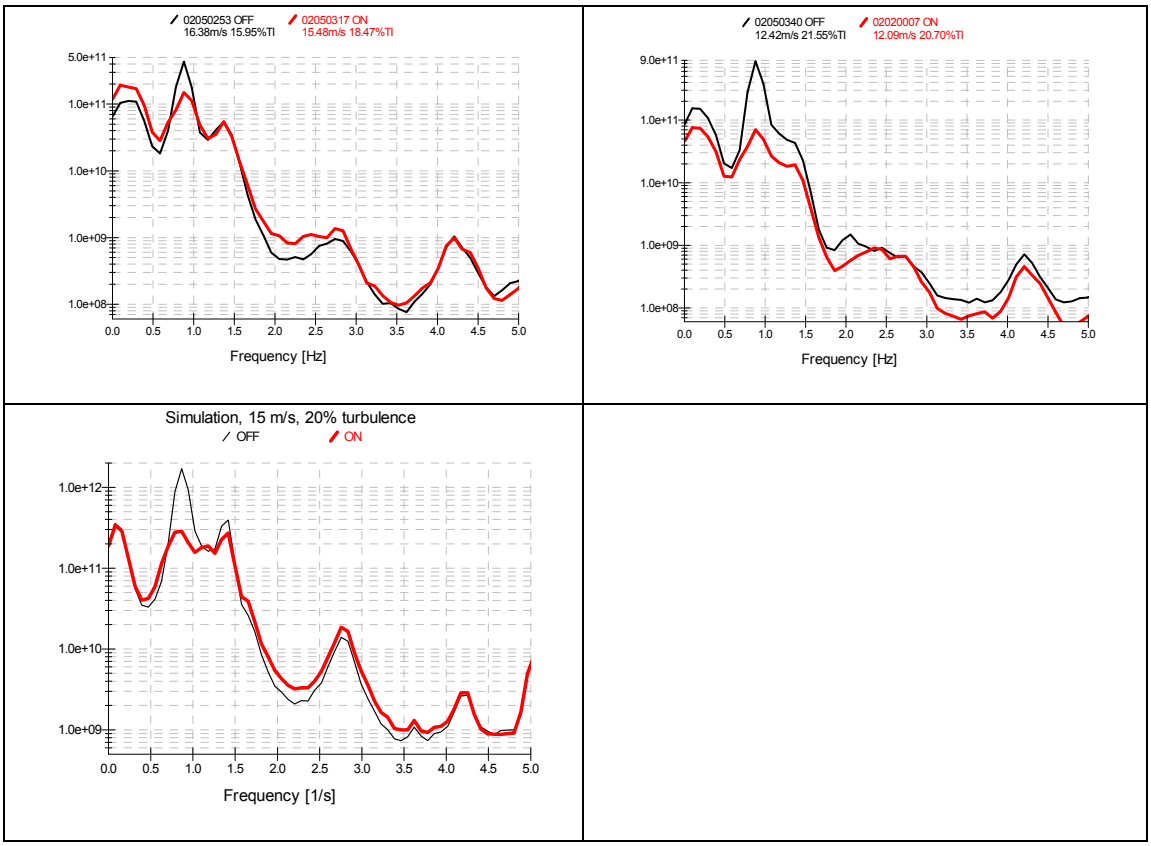

Figure 5. Tower base moment: two comparisons with measured data (top) and a comparable simulation result (bottom). Units: $(Nm)^2/Hz$

Turning to the IPC performance, Figure 6 compares the spectra of blade root out of plane bending moment. The low frequency changes occur for exactly the same reason as for the tower base moment, and the complete removal of the 1P peak at 0.7 Hz is exactly as predicted in simulations, confirming that the IPC is working perfectly as intended.

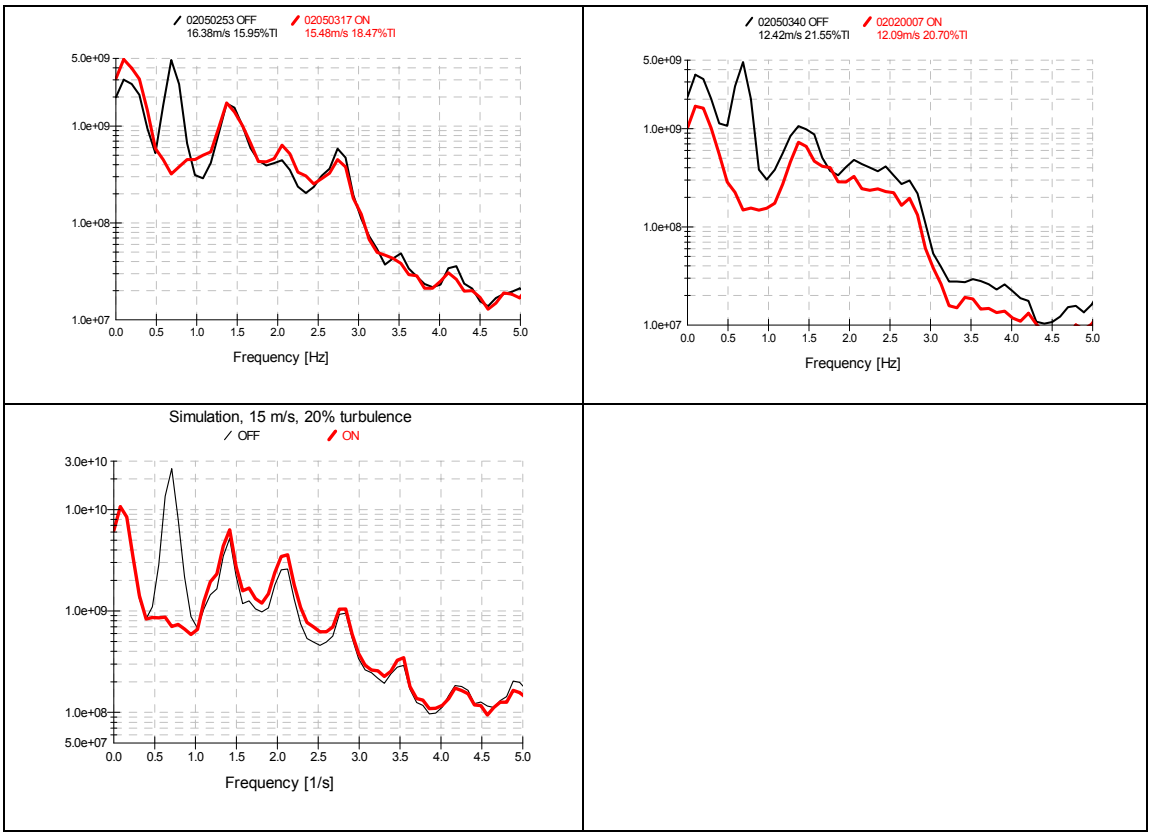

Figure 6. Blade root My moment: two comparisons with measured data (top) and a comparable simulation result (bottom). Units: (Nm)2/Hz

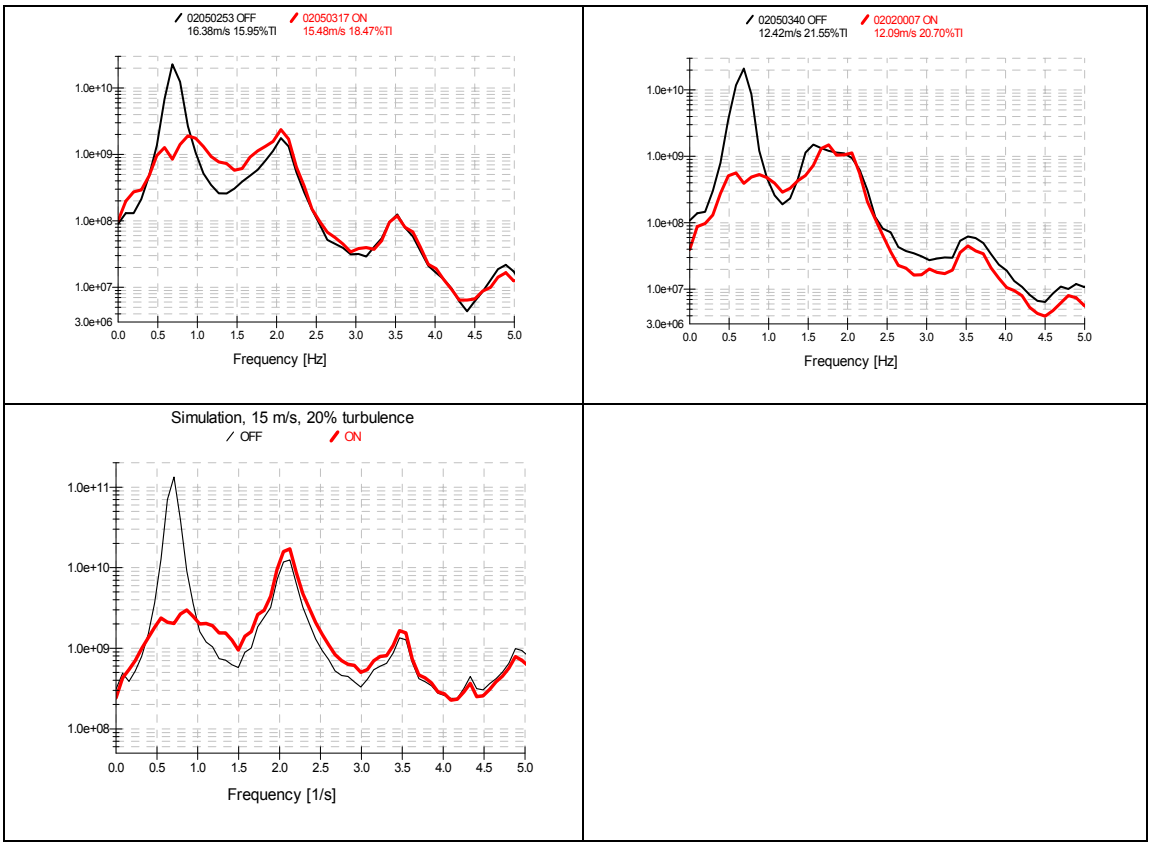

Figure 7. Shaft My moment: two comparisons with measured data (top) and a comparable simulation result (bottom). Units: $(Nm)^2/Hz$

The rotating hub My is calculated as the difference between the out of plane moments at the two blade roots, so the low frequency effects due to gross thrust variations cancel out. This is essentially the main shaft bending moment, and as shown in Figure 7, the dominant 1P load peak is again removed exactly as expected.

The hub fixed Mz or yawing moment is shown in Figure 8 (the fixed My or nodding moment behaves in a very similar way). These moments are normally dominated by the peak at 2P (the blade passing frequency, here 1.4 Hz). As predicted, the IPC successfully removed the 0P (low frequency) and 2P peaks in the non-rotating loads (although in one case, the 0P reduction is small). Unlike in simulation results, there is a clear 1P (once per revolution, here 0.7 Hz) peak in all four datasets, which implies some kind of significant imbalance. There may be some inherent rotor imbalance, but in this special case a likely source of such a large imbalance is the slippage of the teeter brake, shown by the teeter angle plots in Figure 9. The rotor is occasionally knocked to a small teeter angle, where it sticks for a while. Then centrifugal force causes a steady offset in the rotating My, which would appear as a 1P peak in the non-rotating moment. Note that in the 'OFF' case, there are also many periods when the rotor is actually teetering continuously against the brake; these periods might not be expected to contribute to the 1P peak in Mz. Actually, subsequent work has indicated that teeter brake slippage is not sufficient to explain the size of the measured imbalance, which therefore must be due to genuine mass and/or aerodynamic imbalances between the blades.

The IPC is of course achieved at the cost of additional 1P Pitch activity. As Figure 10 shows, this is entirely concentrated at 1P, again agreeing well with simulations. Some short sample time histories of pitch rate are shown in Figure 11. The 1P pitch activity is clearly seen on the ON case. There is also some high frequency noise in both cases.

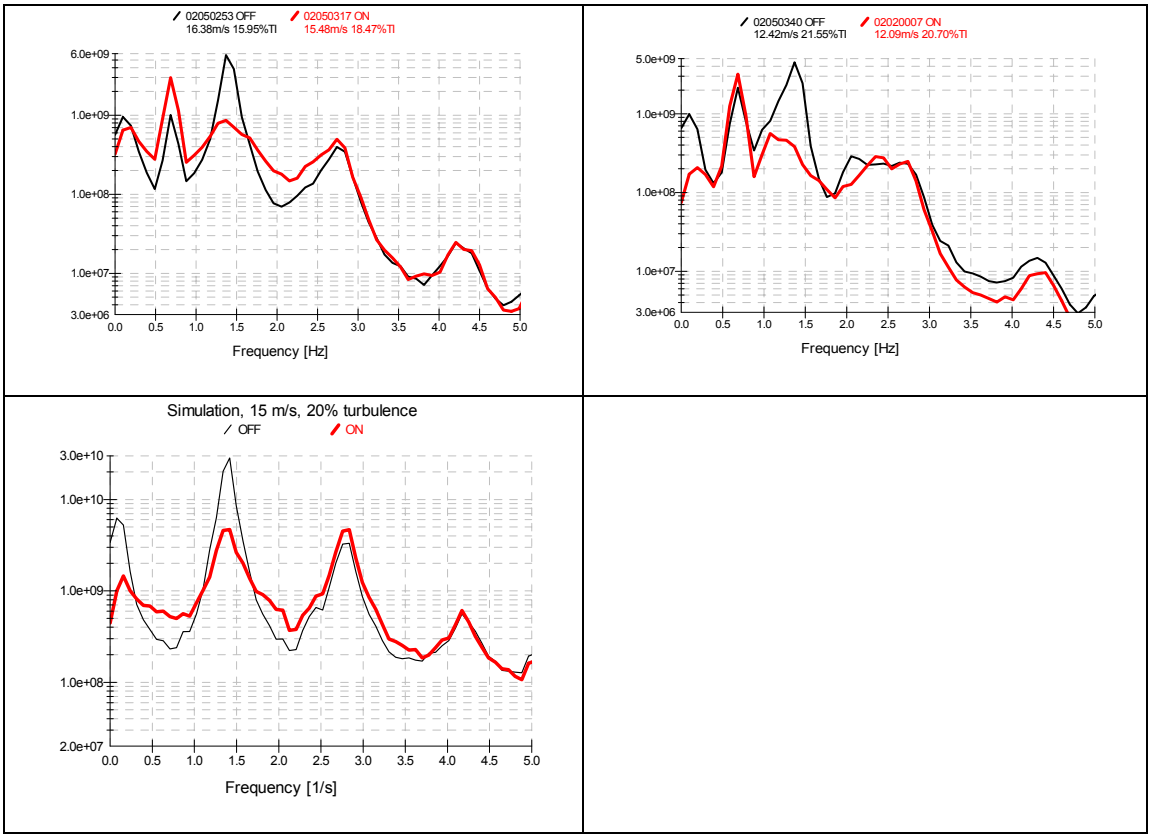

Figure 8. Hub fixed Mz (yaw) moment: two comparisons with measured data (top) and a comparable simulation result (bottom). Units: $(Nm)^2/Hz$

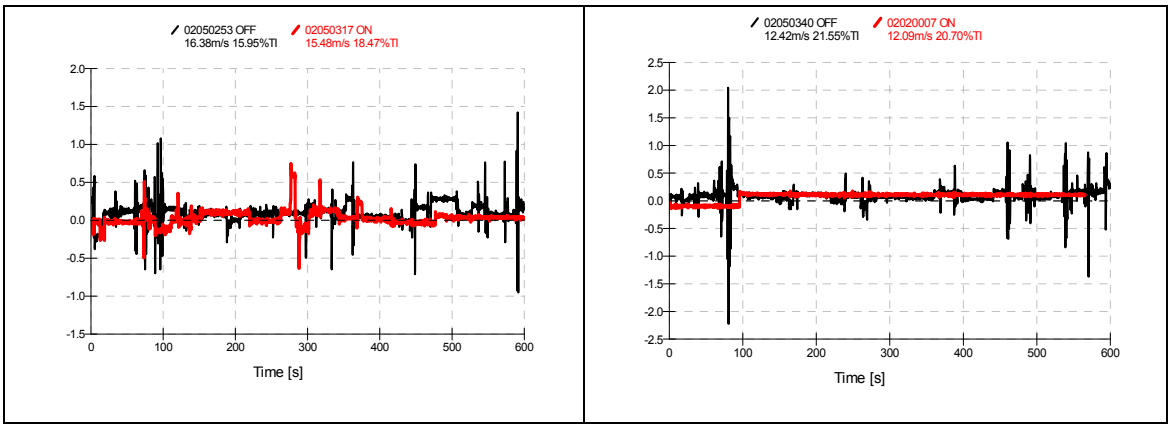

Figure 9. Teeter angles (deg): two comparisons with measured data

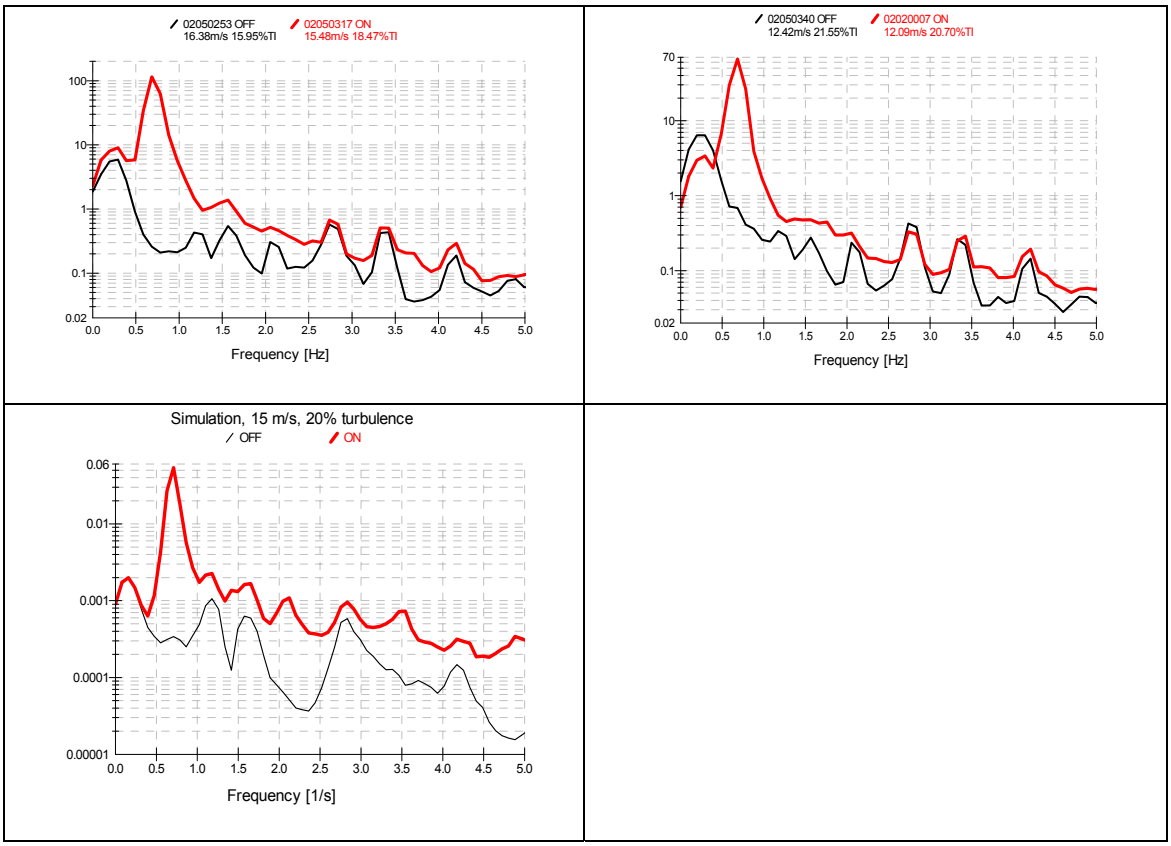

Figure 10. Pitch rate spectra: two comparisons with measured data (top) and a comparable simulation result (bottom). Units: $(rad/s)^2/Hz$

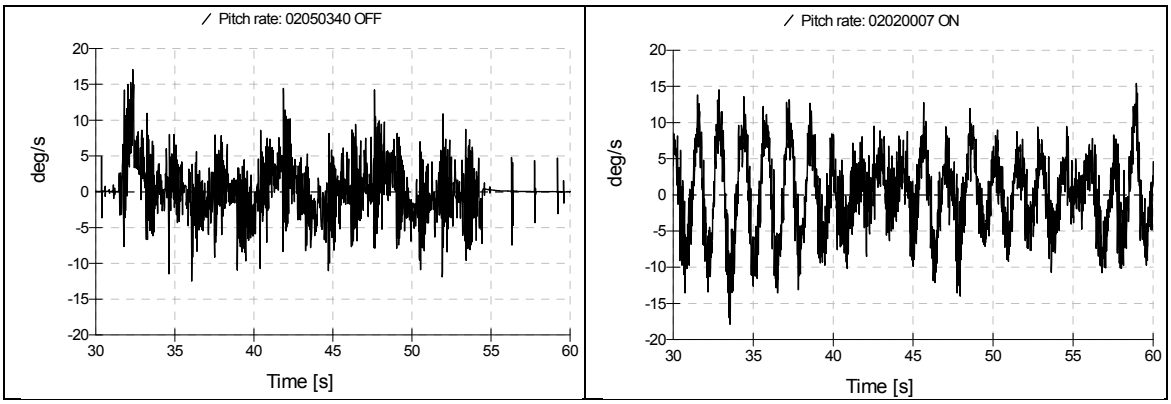

Figure 11. Sample time histories of pitch rate for OFF (left) and ON (right) cases in comparable wind conditions

Below rated, both IPC and FATD cause the pitch to be constantly moving with respect to the optimum 'fine pitch' value, which in principle should cause a small loss of power output. However, simulations have shown any such loss is very small. Since the wind is different for each dataset, it would be very difficult to confirm this from the data in Figure 4 for example. However, this is addressed further in the next section.

Aggregated data analysis

The above results are for just two pair of 10-minute datasets; one without and one with IPC and FATD, chosen because they have similar wind speeds. This demonstrates fairly conclusively that these load reducing features work well, confirming previous

simulation results. For a more complete assessment, a series of 10-minute datasets were processed to estimate the reduction in key damage equivalent loads, and also to confirm that the loss of power production is negligible.
More than 130, 10-minute datasets were collected between 1st February and 13th April 2010. A number were not useful as the wind speed was decreasing, and in some the turbine was only operating for part of the time; although, some extracts of less than 10 minutes were usable. In all, 127 full or partial datasets were used in the analysis presented here.

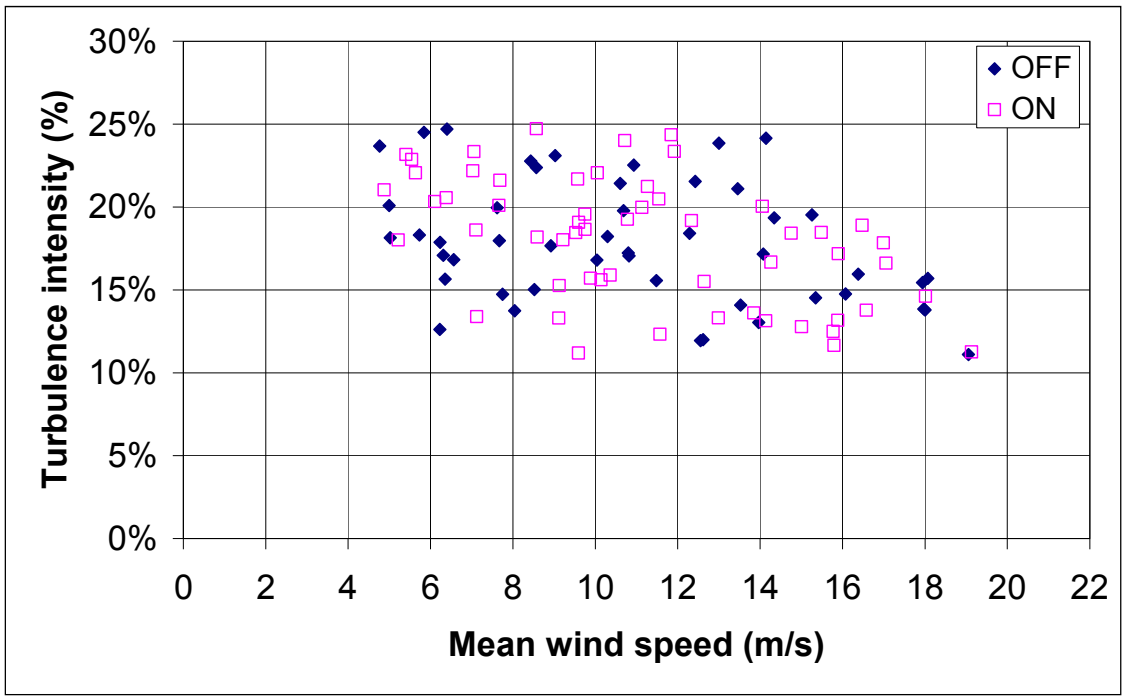

Figure 12: Spread of datasets

For each dataset, the mean wind speed and turbulence intensity at the hub height met mast was calculated. Only datasets with turbulence intensities within the range of 10% - 25% and more than 300s in length were retained. This resulted in 48 datasets with the advanced features OFF and 56 with them ON. The distribution of points is shown in Figure 12.

These datasets were then processed in Bladed to calculate the 1Hz damage equivalent loads as a measure of fatigue damage, using Wöhler exponent 4 (appropriate for steel) or 10 (for GRP composites). (This is the inverse logarithmic slope of the relationship between cycle range and number of cycles to failure, also known as the S-N slope.) Figure 13 clearly shows the reduction in damage equivalent load for the rotating hub My caused by the IPC. For other loads, the reduction is perhaps less clear because of the influence of low-frequency differences, and also the 1P loading due to imbalance and other effects, as mentioned above. Nevertheless, some load reduction is apparent. Figure 14 shows the fixed hub yaw moment Mz, as reduced by IPC, and Figure 15 shows the reduction in tower fore-aft bending caused by FATD.

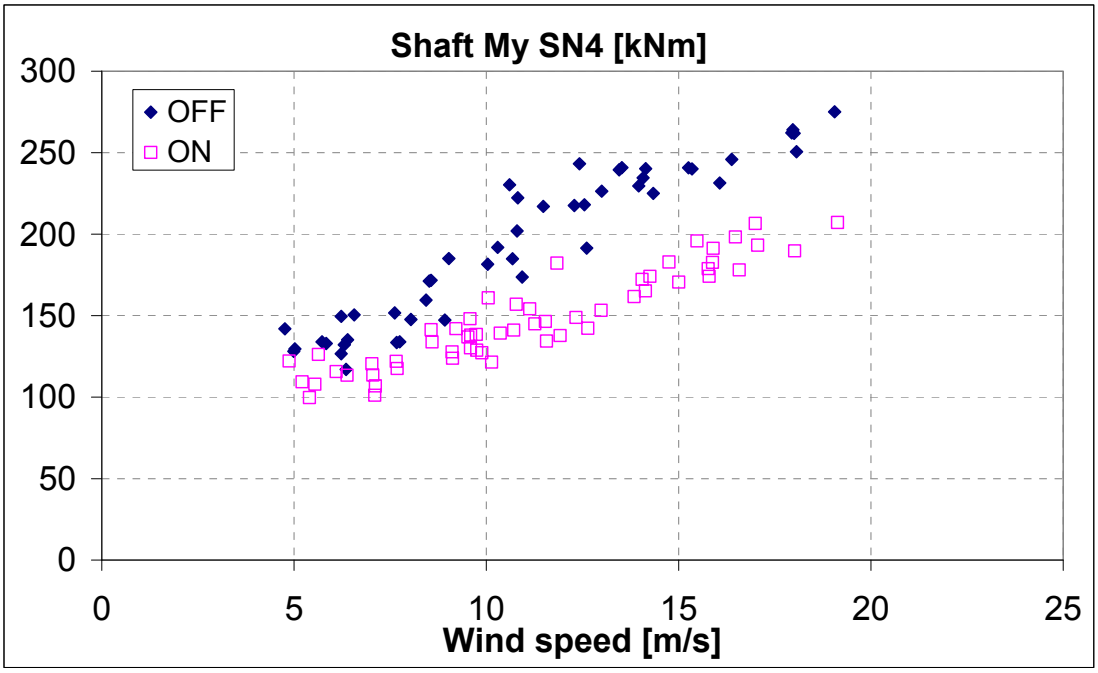

Figure 13. DELs, Hub My

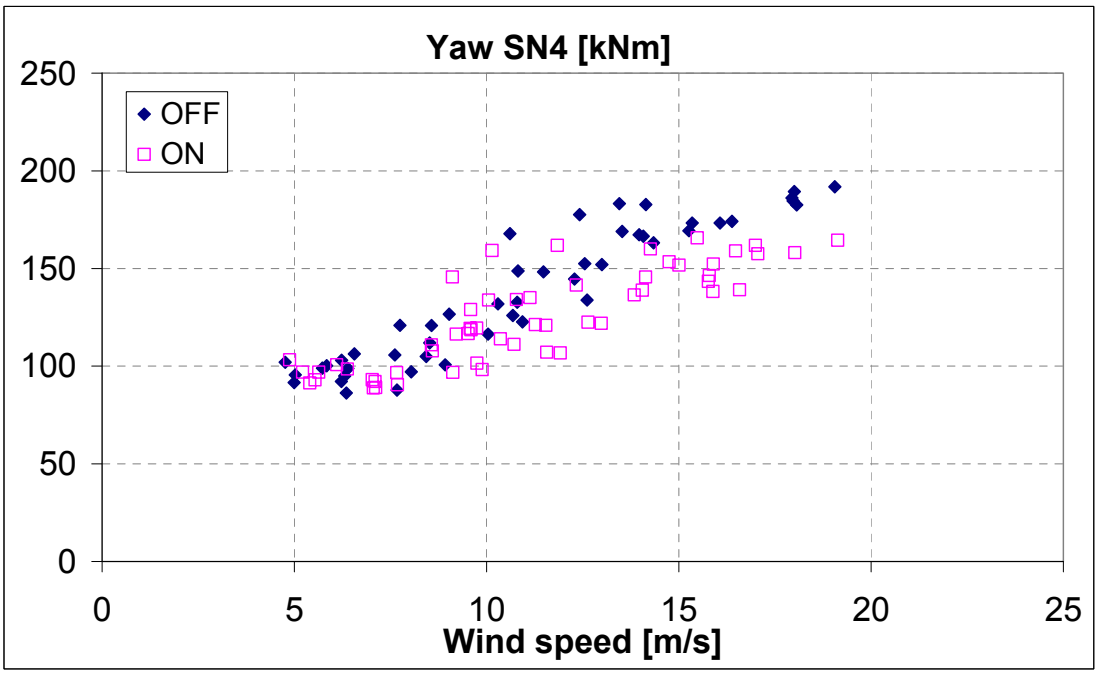

Figure 14. DELs, Hub yaw Mz

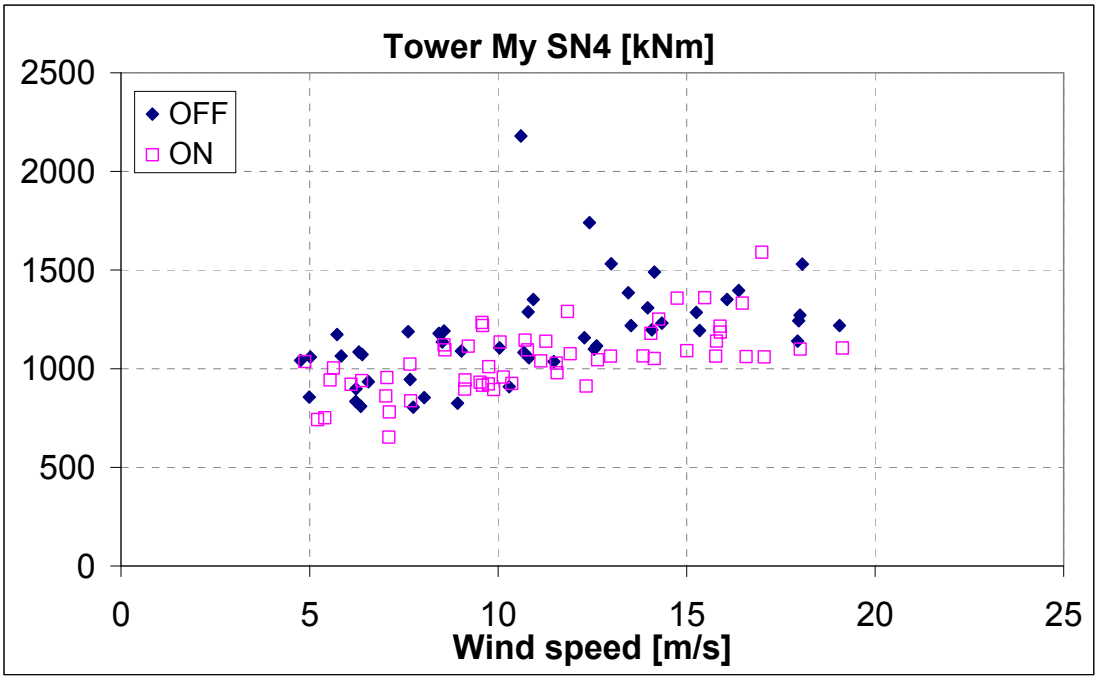

Figure 15. DELs, Tower base My

Finally, in Figure 16, the mean power output for each dataset is plotted, as a check that any loss of power output due to the additional pitch action is small.

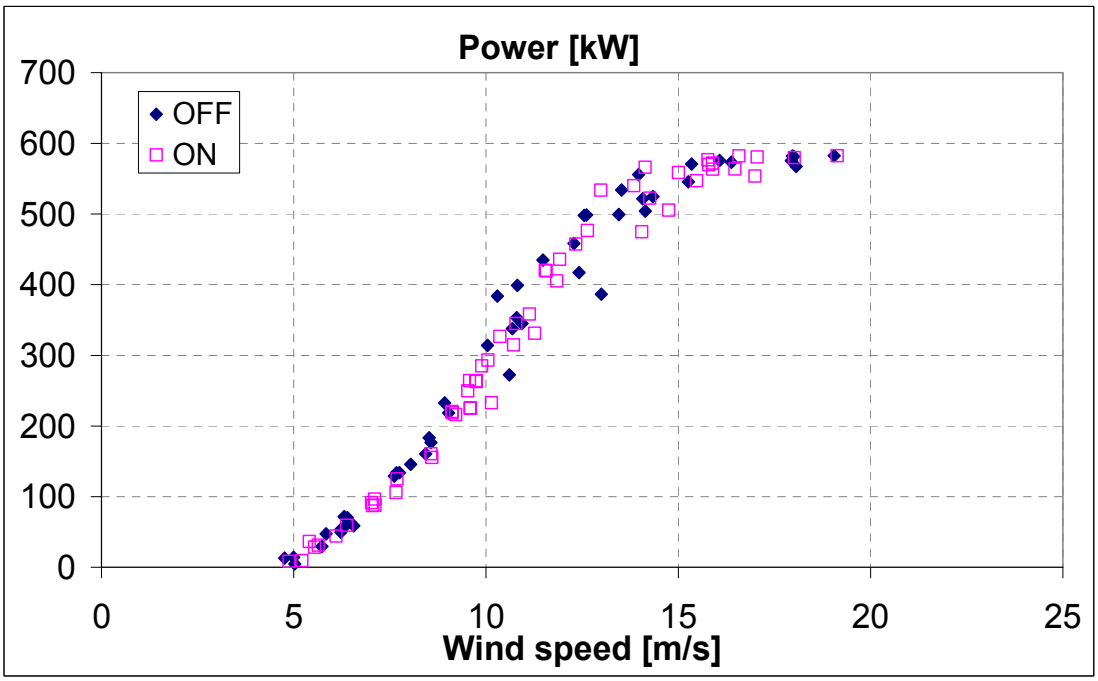

Figure 16: Power output

These graphs clearly have a lot of scatter, so in the following graphs (Figure 17Figure to Figure 22), the results have been binned into 1 m/s wind speed bins. The load reduction trends are now clearly visible.

The number of points in some of the individual bins is too small to allow any measure of statistical significance to be stated. Wider bins would be needed to encompass more points, but some form of normalization is needed to allow bins to be aggregated. The mean percentage damage equivalent load reductions for all eight bins above 12 m/s are shown in Table 4. This comparison includes 20 'OFF' points and 20 'ON' points. The reductions in shaft My and yaw Mz are particularly consistent, with a mean reduction of more than 6 standard deviations.

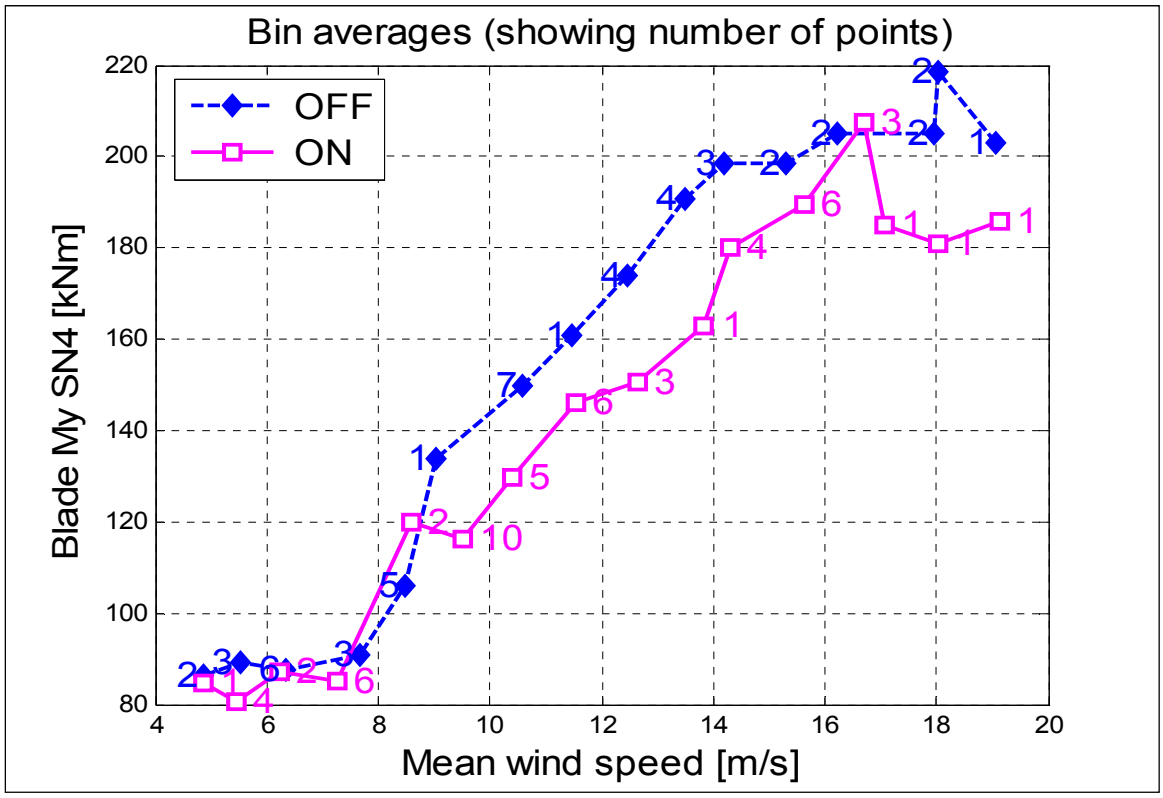

Figure 17. Blade root My DEL (steel)

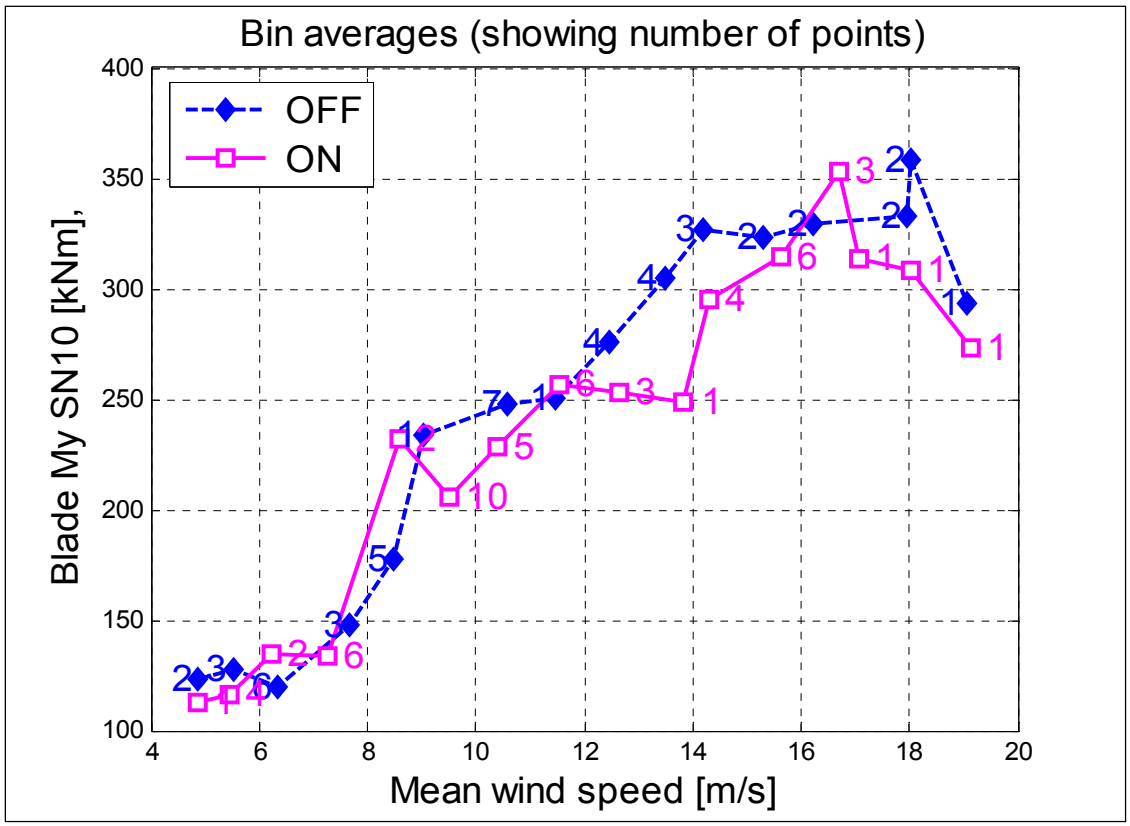

Figure 18. Blade root My DEL (GRP)

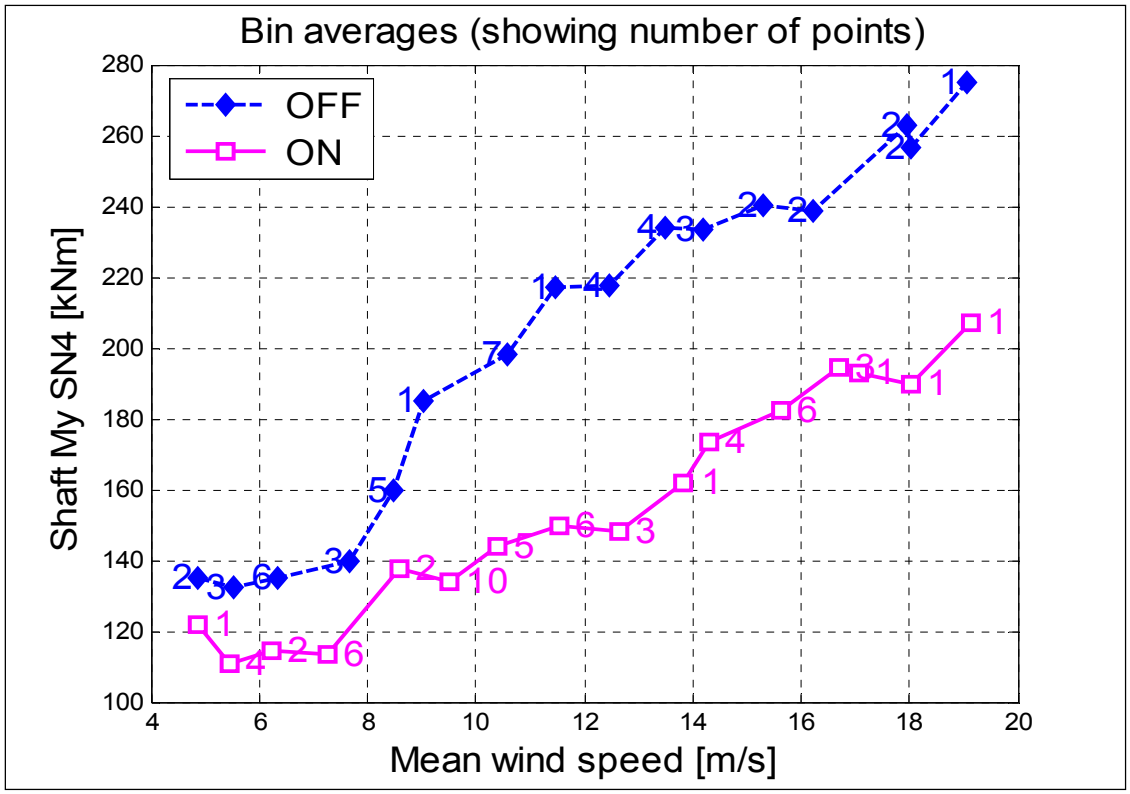

Figure 19. Shaft My DEL (steel)

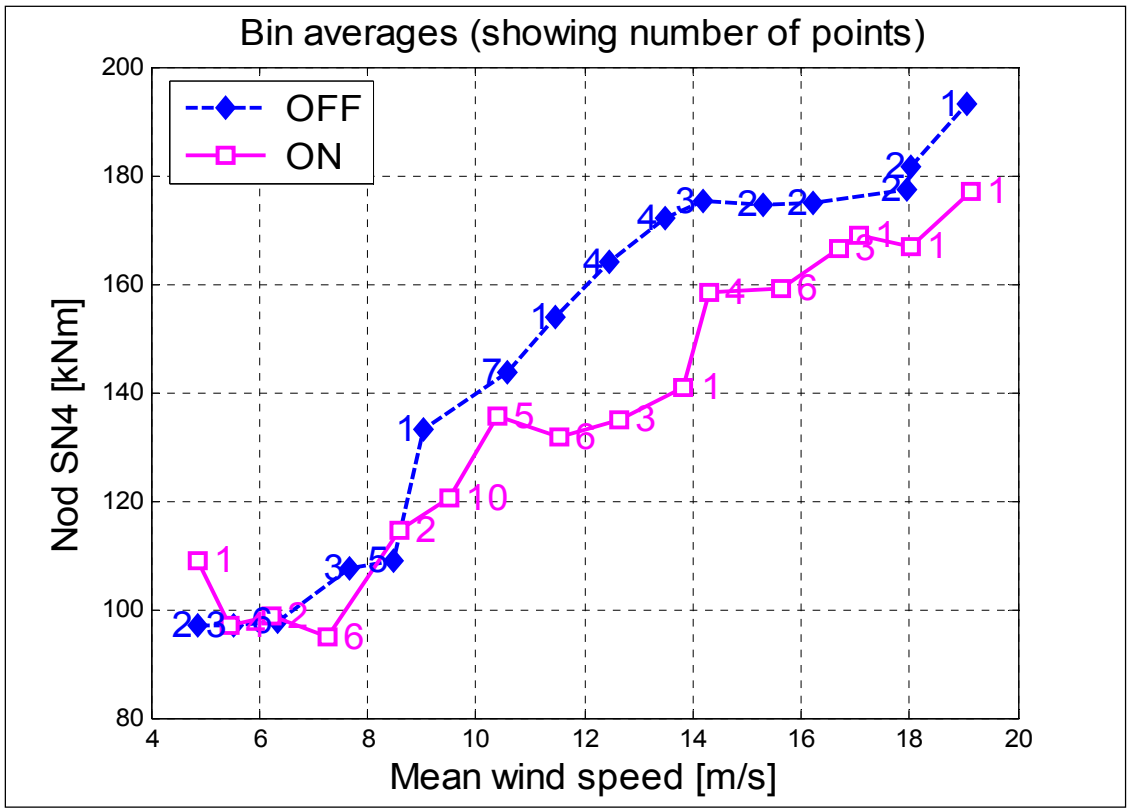

Figure 20. My Nod moment DEL (steel)

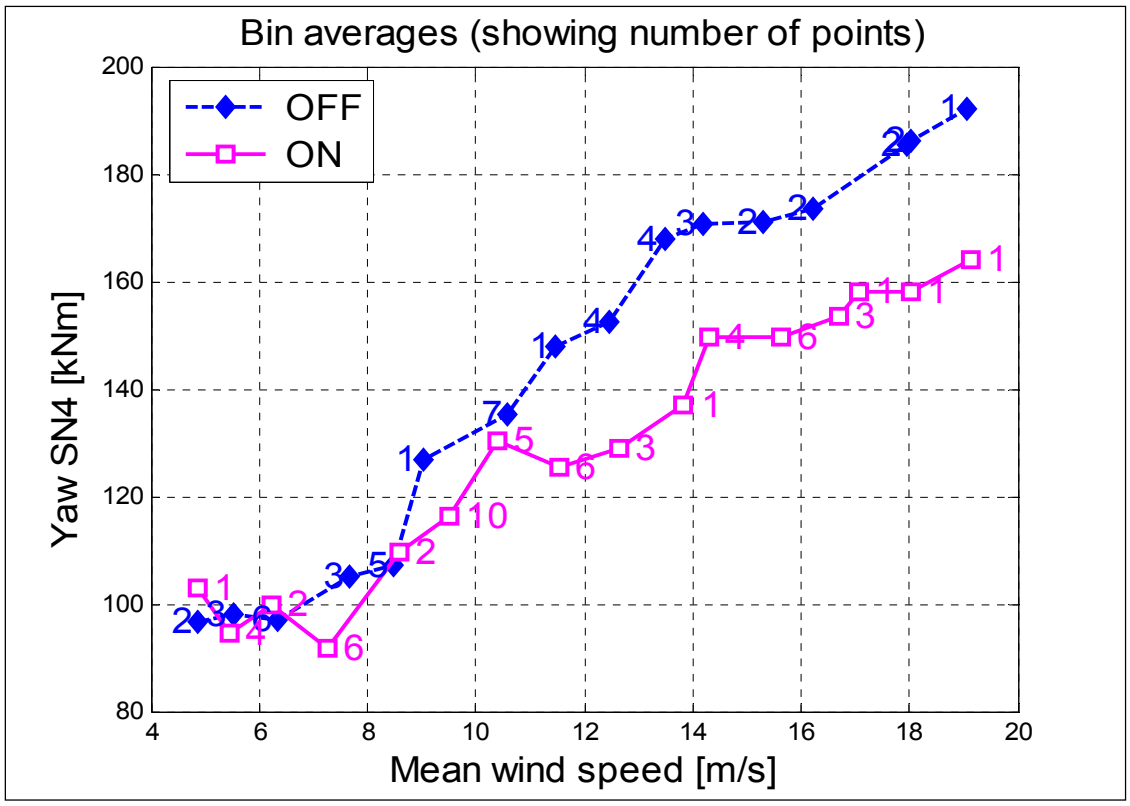

Figure 21. Mz Yaw moment DEL (steel)

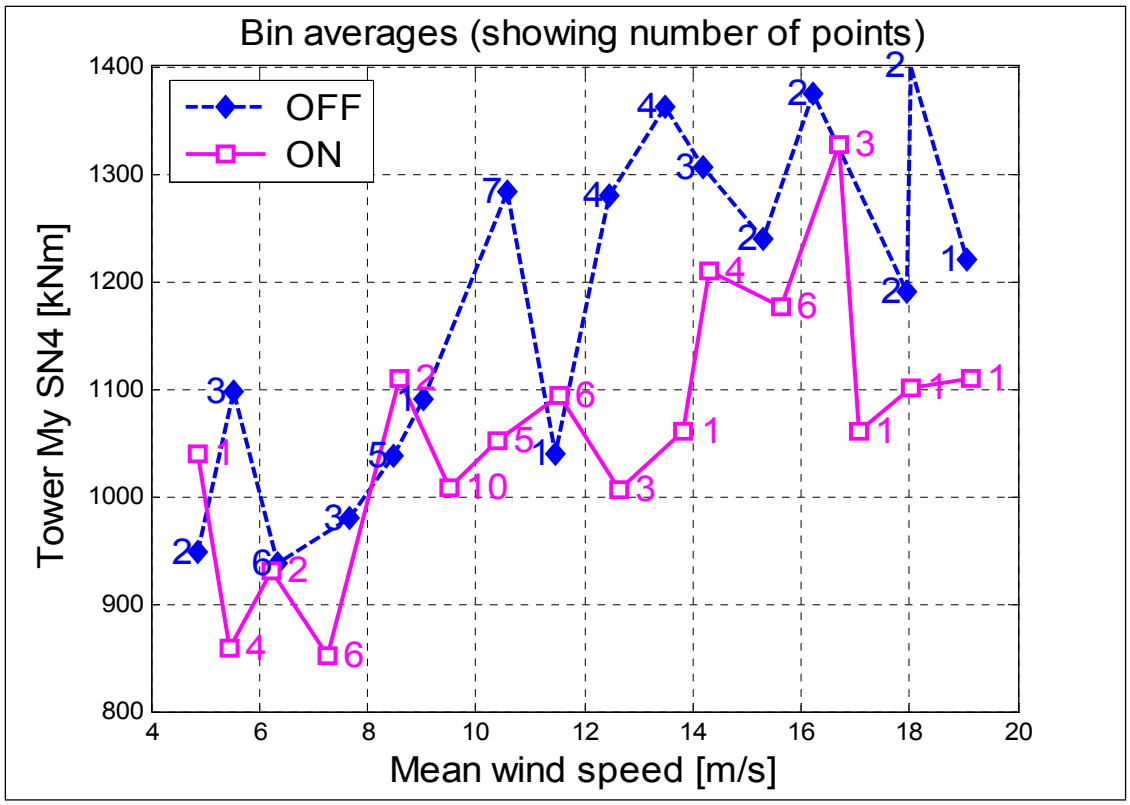

Figure 22. Tower My DEL (steel)

Table 4. Load reductions averaged over the eight bins above 12 m/s

	Mean load reduction	Range	Standard deviation
Blade root My, steel	9.4%	-1.3 to 17.2%	5.9%
Blade root My, GRP	7.3%	-7.4 to 18.3%	7.7%
Shaft My, steel	26.0%	18.5 to 32.0%	4.1%
Nod My, steel	10.0%	4.8 to 18.1%	5.2%
Yaw Mz, steel	14.4%	11.6 to 18.3%	2.1%
Tower My, steel	12.6%	3.5 to 22.2%	7.8%

Figure 23 shows that there is no loss of output above rated – in fact the power seems to be slightly increased in the 12-14 m/s region. In lower winds, there is evidence of a slight decrease in power; but in the normal situation, the IPC would be phased out in low winds anyway, as the loads are lower and the additional pitch action would not be justified.

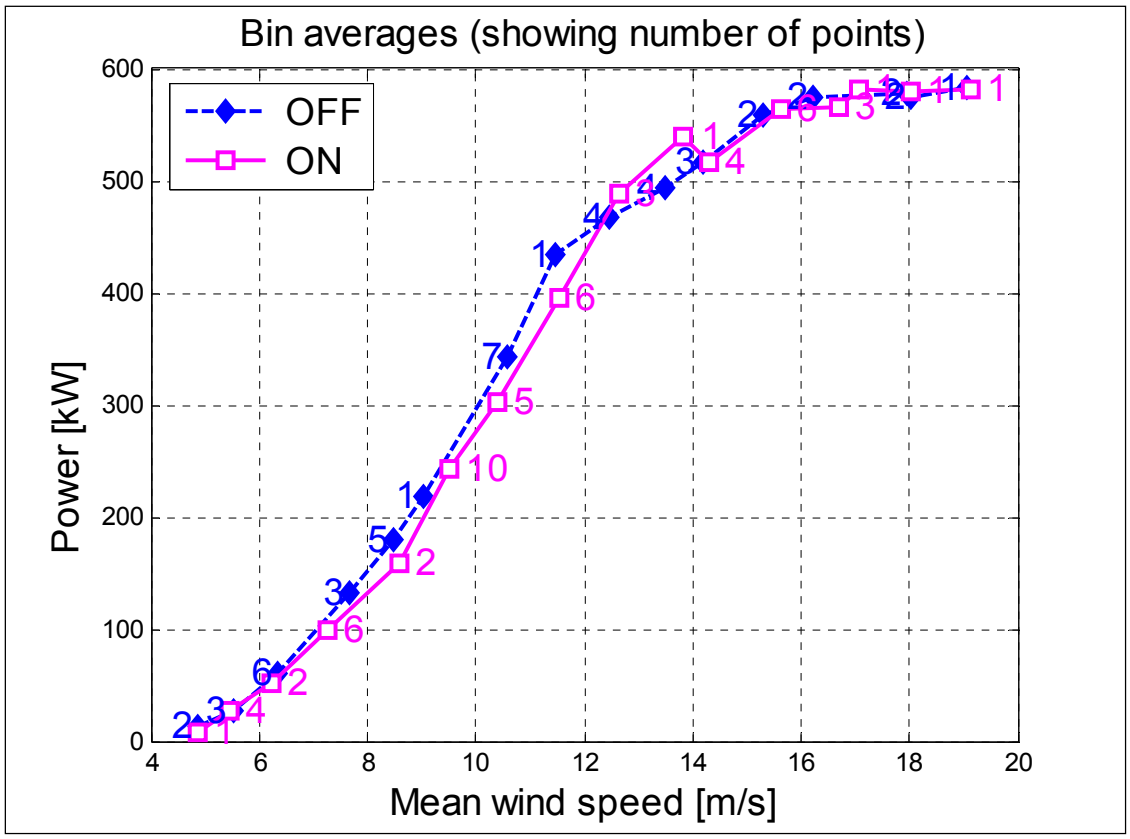

Figure 23: Power output

Conclusions

The data collected from the CART2 field tests clearly shows that both the individual pitch control and the fore-aft tower damping algorithms work as expected, and that the load reductions predicted by simulations can be realised in practice, without significant loss of energy output. The fact that no adjustments of any significance needed to be made to the algorithms or parameter values confirms that these controller features are robust, and should provide the confidence required by turbine designers to be able to use these techniques as an integral part of turbine design in future. Future work includes testing these algorithms on the 3-bladed Controls Advanced Research Turbine to further validate these control approaches for load reduction.

References

1. Developments in Individual Blade Pitch Control, E Bossanyi, "The Science of making Torque from Wind" Delft University of Technology, The Netherlands, April 19-21 2004.

2. Field testing of individual pitch control on the NREL CART-2 wind turbine, E. Bossanyi, A. Wright, proc. European Wind Energy Conference 2009.

3. Further progress with field testing of individual pitch control, E. Bossanyi, A. Wright and P. Fleming, proc. European Wind Energy Conference 2010.

4. Progress with field testing of individual pitch control, E. Bossanyi, A. Wright and P. Fleming, proc. Conference on the science of making torque from wind, The European Academy of Wind Energy, June 2010.

5. Controller field tests on the NREL CART2 turbine, E. Bossanyi, A. Wright and P. Fleming, UPWIND report 11593/BR/08, 22nd June 2010, available at http://www.upwind.eu/Shared%20Documents/WP5%20-%20Publications/D%205.6.1.pdf.

6. Damping of tower motions via pitch control – theory and practice, M. Rossetti, E. Bossanyi, proc. European Wind Energy Conference 2004.

7. Geometry and Structural Properties for the Controls Advanced Research Turbine (CART) from Model Tuning, August 25, 2003–November 30, 2003, K A Stol, NREL/SR-500-32087, http://www.nrel.gov/docs/fy04osti/32087.pdf

8. Wind Turbine Control for Load Reduction, E Bossanyi, Wind Energy 2003 vol 6 pp 229-244.

9. A state-of-the-art controller for the 5MW UPWIND reference wind turbine, E. Bossanyi and D Witcher, Proceedings of European Wind Energy Conference 2009.

10. Controller for 5MW reference turbine, E Bossanyi and D Witcher, Upwind Work Package 5 deliverable report 11593/BR/04, 10th July 2009, http://www.upwind.eu/Shared%20Documents/WP5%20-%20Publications/D%205.1.1.%20Controller%20for%205MW%20reference%20turbine.pdf

Appendix A. Bladed model parameters for CART2

GENERAL CHARACTERISTICS OF ROTOR AND TURBINE

Rotor diameter	42.672	m
Number of blades	2	
Teeter hinge	No	
Hub height	36.8497	m
Offset of hub to side of tower center	0	m
Tower height	34.862	m
Tilt angle of rotor to horizontal	3.77	deg
Cone angle of rotor	0	deg
Blade set angle	0	deg
Rotor overhang	3.858	m
Rotational sense of rotor, viewed from upwind	Clockwise	
Position of rotor relative to tower	Upwind	
Transmission	Gearbox	
Aerodynamic control surfaces	Pitch	
Fixed / Variable speed	Variable	
Diameter of spinner	2.762	m
Radial position of root station	1.381	m
Extension piece diameter	0	m
Extension piece drag coefficient	0	
Cut in windspeed	4	m/s
Cut out windspeed	25	m/s

BLADE GEOMETRY

Blade length	19.955	m
Pre-bend at tip	0	m
Pitch control	Full span	

Distance from root (m)	Chord (m)	Twist (deg)	Twist Axis (% chord)	Thickness (% chord)	Pitch Axis (% chord)	Pre-bend (m)	Aero-dynamic control	Aerofoil section reference
0	1.1929	3.44	50	0	50	0	Pitchable	ART15
0.439	1.1929	3.37	50	0	50	0	Pitchable	ART15
1.0576	1.2689	3.27	49	0	49	0	Pitchable	ART15
1.4967	1.3286	3.2015	47.5	0	47.5	0	Pitchable	ART15
2.2749	1.4058	3.08	45	0	45	0	Pitchable	ART15
2.4944	1.4276	3.0439	44	0	44	0	Pitchable	ART15
3.4921	1.5637	2.88	42.5	0	42.5	0	Pitchable	ART15
4.4899	1.6633	2.7243	40	0	40	0	Pitchable	ART25
4.7094	1.662	2.69	39.5	0	39.5	0	Pitchable	ART25
5.4876	1.6575	2.5414	38.5	0	38.5	0	Pitchable	ART25
6.4853	1.6163	2.354	37.5	0	37.5	0	Pitchable	ART35
7.2636	1.5689	2.21	37.5	0	37.5	0	Pitchable	ART35
7.4831	1.5555	2.1576	37.5	0	37.5	0	Pitchable	ART35
8.4808	1.5017	1.9195	37.5	0	37.5	0	Pitchable	ART45
9.479	1.4274	1.685	37.5	0	37.5	0	Pitchable	ART45
10.476	1.3735	1.4135	37.5	0	37.5	0	Pitchable	ART55
11.075	1.3294	1.24	37.5	0	37.5	0	Pitchable	ART55
11.474	1.3	1.1194	37.5	0	37.5	0	Pitchable	ART55

12.472	1.2461	0.80753	37.5	0	37.5	0	Pitchable	ART65
13.47	1.1718	0.43251	37.5	0	37.5	0	Pitchable	ART65
14.467	1.1179	0.045585	37.5	0	37.5	0	Pitchable	ART75
14.866	1.0885	-0.11	37.5	0	37.5	0	Pitchable	ART75
15.465	1.0444	-0.41931	37.5	0	37.5	0	Pitchable	ART75
16.463	0.9906	-0.93496	37.5	0	37.5	0	Pitchable	ART75-5
17.461	0.9171	-1.4598	37.5	0	37.5	0	Pitchable	ART85
18.458	0.8626	-2.2058	37.5	0	37.5	0	Pitchable	ART85-5
19.456	0.7889	-2.9428	37.5	0	37.5	0	Pitchable	ART95
19.955	0.7889	-3.31	37.5	0	37.5	0	Pitchable	ART95

AEROFOIL DATA

Aerofoil dataset: ART15

Angle of Attack (deg)	Lift coefficient	Drag coefficient
-180	0	0.7384
-170	0.32	0.7409
-160	0.44	0.7961
-150	0.49	0.9
-140	0.54	1.0676
-130	0.53	1.1992
-120	0.46	1.2983
-110	0.36	1.3618
-100	0.25	1.4052
-90	0	1.4439
-80	-0.25	1.4052
-70	-0.36	1.3618
-60	-0.46	1.2983
-50	-0.53	1.1992
-40	-0.54	1.0676
-30	-0.5	0.9
-20	-0.44	0.7961
-10	-0.32	0.7417
-8	-0.26	0.7409
-6	-0.19	0.7403
-4	-0.13	0.7389
-2	-0.06	0.7383
0	0.01	0.7384
2	0.07	0.7384

4	0.14	0.7384
6	0.21	0.7385
8	0.26	0.7402
10	0.32	0.7409
12	0.39	0.7417
14	0.43	0.7428
16	0.45	0.7463
18	0.46	0.7649
20	0.44	0.7961
40	0.54	1.0676
50	0.53	1.1992
60	0.46	1.2983
70	0.36	1.3618
80	0.25	1.4052
90	0	1.4439
100	-0.25	1.4052
110	-0.36	1.3618
120	-0.46	1.2983
130	-0.53	1.1992
140	-0.54	1.0676
150	-0.49	0.9
160	-0.44	0.7961
170	-0.32	0.7409
180	0	0.7384

Aerofoil dataset: ART25

Angle of Attack (deg)	Lift coefficient	Drag coefficient
-180	0.01	0.02
-170	0.72	0.05
-160	0.84	0.31
-150	1.08	0.62
-140	1.15	0.96
-130	1.09	1.3
-120	0.88	1.52
-110	0.6	1.66
-100	0.31	1.76
-90	0	1.8
-80	-0.31	1.76
-70	-0.6	1.66
-60	-0.88	1.52
-50	-1.09	1.3
-40	-1.15	0.96
-30	-1.08	0.62
-20	-0.84	0.31
-10	-0.72	0.017
-8	-0.6	0.0146
-6	-0.54	0.0127
-4	-0.36	0.0086

-2	-0.18	0.0074
0	-0.01	0.0075
2	0.17	0.0077
4	0.35	0.0077
6	0.53	0.0077
8	0.65	0.0127
10	0.82	0.0146
12	0.97	0.017
14	1.05	0.0199
16	1.1	0.0379
18	1.08	0.0948
20	1.04	0.1809
40	1.35	0.875
50	1.33	1.215
60	1.15	1.465
70	0.89	1.625
80	0.6	1.735
90	0.31	1.8
100	-0.31	1.76
110	-0.6	1.66
120	-0.88	1.52
130	-1.09	1.3
140	-1.15	0.96
150	-1.08	0.62
160	-0.84	0.31
170	-0.72	0.05
180	0.01	0.02

Aerofoil dataset: ART35

Angle of Attack (deg)	Lift coefficient	Drag coefficient
-180	-0.06	0.02
-170	0.69	0.05
-160	0.84	0.31
-150	1.08	0.62
-140	1.15	0.96
-130	1.09	1.3
-120	0.88	1.52
-110	0.6	1.66
-100	0.31	1.76
-90	0	1.8
-80	-0.31	1.76
-70	-0.6	1.66
-60	-0.88	1.52
-50	-1.09	1.3
-40	-1.15	0.96
-30	-1.08	0.62
-20	-0.84	0.31
-10	-0.69	0.0166

-8	-0.55	0.0144
-6	-0.44	0.0119
-4	-0.27	0.0089
-2	-0.11	0.0071
0	0.06	0.0074
2	0.22	0.0075
4	0.38	0.0075
6	0.55	0.0084
8	0.69	0.0124
10	0.87	0.0144
12	1.02	0.0166
14	1.13	0.0192
16	1.18	0.0406
18	1.18	0.1012
20	1.13	0.1901
40	1.32	0.8818
50	1.29	1.2218
60	1.12	1.4694
70	0.85	1.6278
80	0.57	1.737
90	0.28	1.8
100	-0.31	1.76
110	-0.6	1.66
120	-0.88	1.52
130	-1.09	1.3
140	-1.15	0.96
150	-1.08	0.62
160	-0.84	0.31
170	-0.69	0.05
180	-0.06	0.02

Aerofoil dataset: ART45

Angle of Attack (deg)	Lift coefficient	Drag coefficient
-180	-0.12	0.02
-170	0.58	0.05
-160	0.84	0.31
-150	1.08	0.62
-140	1.15	0.96
-130	1.09	1.3
-120	0.88	1.52
-110	0.6	1.66
-100	0.31	1.76
-90	0	1.8
-80	-0.31	1.76
-70	-0.6	1.66
-60	-0.88	1.52
-50	-1.09	1.3
-40	-1.15	0.96

-30	-1.08	0.62
-20	-0.84	0.31
-10	-0.58	0.0142
-8	-0.42	0.0123
-6	-0.34	0.0111
-4	-0.19	0.0092
-2	-0.04	0.0068
0	0.12	0.0074
2	0.27	0.0073
4	0.42	0.0073
6	0.58	0.0095
8	0.74	0.0123
10	0.92	0.0142
12	1.09	0.0163
14	1.2	0.0187
16	1.27	0.0453
18	1.27	0.1115
20	1.2	0.2042
40	1.29	0.892
50	1.25	1.232
60	1.07	1.476
70	0.81	1.632
80	0.52	1.74
90	0.23	1.8
100	-0.31	1.76
110	-0.6	1.66
120	-0.88	1.52
130	-1.09	1.3
140	-1.15	0.96
150	-1.08	0.62
160	-0.84	0.31
170	-0.58	0.05
180	-0.12	0.02

Aerofoil dataset: ART55

Angle of Attack (deg)	Lift coefficient	Drag coefficient
-180	-0.17	0.02
-170	0.64	0.05
-160	0.84	0.31
-150	1.08	0.62
-140	1.15	0.96
-130	1.09	1.3
-120	0.88	1.52
-110	0.6	1.66
-100	0.31	1.76
-90	0	1.8
-80	-0.31	1.76
-70	-0.6	1.66

-60	-0.88	1.52
-50	-1.09	1.3
-40	-1.15	0.96
-30	-1.08	0.62
-20	-0.84	0.31
-10	-0.64	0.0144
-8	-0.48	0.0124
-6	-0.29	0.0104
-4	-0.14	0.0093
-2	0.02	0.007
0	0.17	0.0074
2	0.33	0.0072
4	0.48	0.0076
6	0.64	0.0105
8	0.82	0.0124
10	0.99	0.0144
12	1.15	0.0166
14	1.26	0.0214
16	1.32	0.0566
18	1.31	0.1289
20	1.19	0.2249
40	1.26	0.9056
50	1.22	1.2456
60	1.04	1.4848
70	0.77	1.6376
80	0.48	1.744
90	0.19	1.8
100	-0.31	1.76
110	-0.6	1.66
120	-0.88	1.52
130	-1.09	1.3
140	-1.15	0.96
150	-1.08	0.62
160	-0.84	0.31
170	-0.64	0.05
180	-0.17	0.02

Aerofoil dataset: ART65

Angle of Attack (deg)	Lift coefficient	Drag coefficient
-180	-0.21	0.02
-170	0.69	0.05
-160	0.84	0.31
-150	1.08	0.62
-140	1.15	0.96
-130	1.09	1.3
-120	0.88	1.52
-110	0.6	1.66
-100	0.31	1.76

-90	0	1.8
-80	-0.31	1.76
-70	-0.6	1.66
-60	-0.88	1.52
-50	-1.09	1.3
-40	-1.15	0.96
-30	-1.08	0.62
-20	-0.84	0.31
-10	-0.69	0.0128
-8	-0.5	0.0111
-6	-0.35	0.01
-4	-0.16	0.0088
-2	0.02	0.0084
0	0.21	0.0073
2	0.4	0.0075
4	0.59	0.0081
6	0.78	0.0111
8	0.94	0.0128
10	1.08	0.0159
12	1.19	0.0184
14	1.26	0.0268
16	1.27	0.0727
18	1.21	0.1519
20	1.06	0.2514
40	1.25	0.9226
50	1.2	1.2626
60	1.01	1.4958
70	0.73	1.6446
80	0.44	1.749
90	0.15	1.8
100	-0.31	1.76
110	-0.6	1.66
120	-0.88	1.52
130	-1.09	1.3
140	-1.15	0.96
150	-1.08	0.62
160	-0.84	0.31
170	-0.69	0.05
180	-0.21	0.02

Aerofoil dataset: ART75

Angle of Attack (deg)	Lift coefficient	Drag coefficient
-180	-0.26	0.02
-170	0.67	0.05
-160	0.84	0.31
-150	1.08	0.62
-140	1.15	0.96
-130	1.09	1.3

-120	0.88	1.52
-110	0.6	1.66
-100	0.31	1.76
-90	0	1.8
-80	-0.31	1.76
-70	-0.6	1.66
-60	-0.88	1.52
-50	-1.09	1.3
-40	-1.15	0.96
-30	-1.08	0.62
-20	-0.84	0.31
-10	-0.67	0.0116
-8	-0.47	0.0097
-6	-0.34	0.0085
-4	-0.14	0.0079
-2	0.06	0.0071
0	0.26	0.007
2	0.47	0.0076
4	0.67	0.0097
6	0.87	0.0116
8	1.05	0.0134
10	1.18	0.0155
12	1.27	0.0191
14	1.34	0.0371
16	1.33	0.0942
18	1.24	0.1806
20	1.03	0.2833
40	1.23	0.943
50	1.18	1.283
60	0.98	1.509
70	0.7	1.653
80	0.41	1.755
90	0.12	1.8
100	-0.31	1.76
110	-0.6	1.66
120	-0.88	1.52
130	-1.09	1.3
140	-1.15	0.96
150	-1.08	0.62
160	-0.84	0.31
170	-0.67	0.05
180	-0.26	0.02

Aerofoil dataset: ART75-5

Angle of Attack (deg)	Lift coefficient	Drag coefficient
-180	-0.3	0.02
-170	0.71	0.05
-160	0.84	0.31

-150	1.08	0.62
-140	1.15	0.96
-130	1.09	1.3
-120	0.88	1.52
-110	0.6	1.66
-100	0.31	1.76
-90	0	1.8
-80	-0.31	1.76
-70	-0.6	1.66
-60	-0.88	1.52
-50	-1.09	1.3
-40	-1.15	0.96
-30	-1.08	0.62
-20	-0.84	0.31
-10	-0.71	0.0116
-8	-0.51	0.0097
-6	-0.32	0.0085
-4	-0.12	0.0079
-2	0.1	0.0071
0	0.3	0.007
2	0.51	0.0076
4	0.71	0.0097
6	0.92	0.0116
8	1.1	0.0134
10	1.24	0.0155
12	1.33	0.0191
14	1.39	0.0371
16	1.38	0.0942
18	1.27	0.1806
20	1.01	0.2833
40	1.21	0.943
50	1.16	1.283
60	0.96	1.509
70	0.68	1.653
80	0.4	1.755
90	0.1	1.8
100	-0.31	1.76
110	-0.6	1.66
120	-0.88	1.52
130	-1.09	1.3
140	-1.15	0.96
150	-1.08	0.62
160	-0.84	0.31
170	-0.67	0.05
180	-0.3	0.02

Aerofoil dataset: ART85

Angle of Attack (deg)	Lift coefficient	Drag coefficient

-180	-0.33	0.02
-170	0.75	0.05
-160	0.84	0.31
-150	1.08	0.62
-140	1.15	0.96
-130	1.09	1.3
-120	0.88	1.52
-110	0.6	1.66
-100	0.31	1.76
-90	0	1.8
-80	-0.31	1.76
-70	-0.6	1.66
-60	-0.88	1.52
-50	-1.09	1.3
-40	-1.15	0.96
-30	-1.08	0.62
-20	-0.84	0.31
-10	-0.75	0.0116
-8	-0.55	0.0097
-6	-0.3	0.0085
-4	-0.09	0.0079
-2	0.13	0.0071
0	0.33	0.007
2	0.55	0.0076
4	0.75	0.0097
6	0.96	0.0116
8	1.15	0.0134
10	1.29	0.0155
12	1.38	0.0191
14	1.43	0.0371
16	1.42	0.0942
18	1.29	0.1806
20	0.99	0.2833
40	1.2	0.943
50	1.15	1.283
60	0.94	1.509
70	0.67	1.653
80	0.38	1.755
90	0.09	1.8
100	-0.31	1.76
110	-0.6	1.66
120	-0.88	1.52
130	-1.09	1.3
140	-1.15	0.96
150	-1.08	0.62
160	-0.84	0.31
170	-0.75	0.05
180	-0.33	0.02

Aerofoil dataset: ART85-5

Angle of Attack (deg)	Lift coefficient	Drag coefficient
-180	-0.38	0.02
-170	0.7	0.05
-160	0.84	0.31
-150	1.08	0.62
-140	1.15	0.96
-130	1.09	1.3
-120	0.88	1.52
-110	0.6	1.66
-100	0.31	1.76
-90	0	1.8
-80	-0.31	1.76
-70	-0.6	1.66
-60	-0.88	1.52
-50	-1.09	1.3
-40	-1.15	0.96
-30	-1.08	0.62
-20	-0.84	0.31
-10	-0.7	0.0116
-8	-0.49	0.0097
-6	-0.27	0.0085
-4	-0.05	0.0079
-2	0.17	0.0071
0	0.38	0.007
2	0.6	0.0076
4	0.8	0.0097
6	1.01	0.0116
8	1.21	0.0134
10	1.29	0.0155
12	1.36	0.0191
14	1.49	0.0371
16	1.46	0.0942
18	1.31	0.1806
20	0.94	0.2833
40	1.18	0.943
50	1.13	1.283
60	0.92	1.509
70	0.64	1.653
80	0.35	1.755
90	0.06	1.8
100	-0.31	1.76
110	-0.6	1.66
120	-0.88	1.52
130	-1.09	1.3
140	-1.15	0.96
150	-1.08	0.62

160	-0.84	0.31
170	-0.75	0.05
180	-0.38	0.02

Aerofoil dataset: ART95

Angle of Attack (deg)	Lift coefficient	Drag coefficient
-180	-0.42	0.02
-170	0.64	0.05
-160	0.84	0.31
-150	1.08	0.62
-140	1.15	0.96
-130	1.09	1.3
-120	0.88	1.52
-110	0.6	1.66
-100	0.31	1.76
-90	0	1.8
-80	-0.31	1.76
-70	-0.6	1.66
-60	-0.88	1.52
-50	-1.09	1.3
-40	-1.15	0.96
-30	-1.08	0.62
-20	-0.84	0.31
-10	-0.64	0.0116
-8	-0.42	0.0098
-6	-0.23	0.0078
-4	-0.01	0.0073
-2	0.21	0.0063
0	0.42	0.0065
2	0.64	0.0077
4	0.85	0.0098
6	1.06	0.0116
8	1.26	0.0135
10	1.42	0.0163
12	1.5	0.0197
14	1.54	0.0452
16	1.5	0.1095
18	1.32	0.2003
20	0.88	0.3047
40	1.16	0.9566
50	1.1	1.2966
60	0.89	1.5178
70	0.61	1.6586
80	0.32	1.759
90	0.03	1.8
100	-0.31	1.76
110	-0.6	1.66
120	-0.88	1.52

130	-1.09	1.3
140	-1.15	0.96
150	-1.08	0.62
160	-0.84	0.31
170	-0.64	0.05
180	-0.42	0.02

BLADE MASS DISTRIBUTION

Distance from root (m)	Centre of Mass (% chord)	Mass/unit length (kg/m)
0	50	282.92
0.439	50	290.24
1.0576	50	261.88
1.4967	50	240.02
2.2749	50	201.28
2.4944	50	198.62
3.4921	50	186.52
4.4899	50	172.24
4.7094	50	169.1
5.4876	50	156.83
6.4853	50	142.84
7.2636	50	133.19
7.4831	50	129.45
8.4808	50	112.42
9.479	50	100.58
10.476	50	87.145
11.075	50	78.57
11.474	50	74.273
12.472	50	63.352
13.47	50	51.359
14.467	50	41.429
14.866	50	37.59
15.465	50	31.694
16.463	50	22.761
17.461	50	15.842
18.458	50	11.652
19.456	50	7.8599
19.955	50	6.02

Blade Mass Integrals

Blade Mass	2126.19	kg
First Mass Moment	12408.7	kgm
Second Mass Moment	115269	kgm²
Blade inertia about shaft	153597	kgm²

BLADE STIFFNESS DISTRIBUTION

Radial Position (m)	Flapwise stiffness (Nm²)	Edgewise stiffness (Nm²)

0	1.65E+08	2.83E+08
0.439	1.61E+08	3.18E+08
1.0576	1.42E+08	3.28E+08
1.4967	1.264E+08	3.204E+08
2.2749	9.87E+07	3.07E+08
2.4944	9.504E+07	3.13E+08
3.4921	7.84E+07	3.4E+08
4.4899	6.266E+07	3.416E+08
4.7094	5.92E+07	3.42E+08
5.4876	5.066E+07	3.024E+08
6.4853	4.088E+07	2.616E+08
7.2636	3.41E+07	2.37E+08
7.4831	3.251E+07	2.251E+08
8.4808	2.529E+07	1.712E+08
9.479	1.968E+07	1.458E+08
10.476	1.493E+07	1.146E+08
11.075	1.23E+07	9.4E+07
11.474	1.1E+07	8.718E+07
12.472	7.857E+06	6.968E+07
13.47	5.474E+06	4.952E+07
14.467	3.693E+06	3.708E+07
14.866	3.02E+06	3.26E+07
15.465	2.364E+06	2.623E+07
16.463	1.432E+06	1.75E+07
17.461	855310	1.287E+07
18.458	537870	9.575E+06
19.456	310180	7.601E+06
19.955	209000	6.8E+06

HUB MASS AND INERTIA

Mass of hub	5852	kg
Mass centre of hub	-0.21	m
Hub inertia: about shaft	15000	kgm²
perpendicular to shaft	0	kgm²
Total Rotor Mass	10104.4	kg
Total Rotor Inertia	322193	kgm²

TOWER DETAILS

Station Number	Height (m)	Diameter (m)	Mass/unit length (kg/m)	Stiffness (Nm²)
1	0	4.42	1548	8.21E+10
2	2.29392	3.86647	1361	5.48E+10
3	6.86781	2.76277	1428	2.96E+10
4	9.1443	2.21344	1311	1.75E+10
5	11.4801	2.2	1311	1.75E+10
6	14.9872	2.2	1311	1.75E+10
7	17.9086	2.2	878	1.14E+10
8	21.4157	2.2	878	1.14E+10

9	24.3407	2.2	878	1.14E+10
10	27.2481	2.2	599	7.63E+09
11	30.7274	2.2	599	7.63E+09
12	33.6628	2.2	1311	1.75E+10
13	34.862	2.2	1311	1.75E+10

Total Tower Mass	37944	kg
Total Turbine Mass	77161.4	kg

Drag coefficient for tower	0
Environment	Land
Foundation	Rigid

NACELLE MASS

Nacelle mass	29113	kg
Nacelle centre of mass lateral offset	0	m
Nacelle centre of mass above tower top	1.734	m
Nacelle centre of mass in front of tower axis	1.1	m
Yaw inertia (about tower axis)	71750	kgm²
Nodding inertia (about CoG)	0	kgm²
Rolling inertia (about CoG)	0	kgm²
Total Tower-head Mass	39217.4	kg
Total Yaw Inertia: 0° azimuth	212921	kgm²
Total Yaw Inertia: 90° azimuth	535114	kgm²

DRIVE TRAIN

Gearbox ratio	43.165	
Position of shaft brake	High speed shaft	(Gearbox End)
Generator inertia	34.4	kgm²
High speed shaft inertia:	0	kgm²
Low speed shaft	Flexible	
Low speed shaft torsional stiffness	2.691E+07	Nm/rad
Low speed shaft torsional damping	0	Nms/rad
High speed shaft	Stiff	

GENERATOR CHARACTERISTICS

Generator model	Variable Speed	
Power electronics time constant	0	s
Maximum generator torque	4000	Nm
Minimum generator torque	0	Nm
Phase Angle	0	deg

Discrete Controller: Signal noise

Blade pitch angle discretisation step	0	deg
Electrical power discretisation step	0	kW
Generator speed discretisation step	0	rpm

Rotor speed discretisation step	0	rpm
Generator torque discretisation step	0	Nm
Yaw error (wind vane) discretisation step	0	deg
Nacelle wind speed discretisation step	0	m/s
Nacelle direction discretisation step	0	deg
Blade OPBM discretisation step	5600	Nm
Fore-aft acceleration discretisation step	0	m/s²
Side-side acceleration discretisation step	0	m/s²
Rotor azimuth discretisation step	0	deg
Random number seed	0	

PITCH ACTUATOR

Pitch actuator responds to	Rate demand	
Pitch Rate response	Passive	
First order lag time constant	0.016667	s
Lower pitch limit	-10	deg
Upper pitch limit	90	deg
Lower pitch rate limit	-18	deg/s
Upper pitch rate limit	18	deg/s
Pitch actuation	Individual	

MODAL ANALYSIS (uncoupled component modes)

Rotor modes at 0.0 degrees pitch

Mode	Frequency at 42.0 rpm (Hz)	Non-rotating frequency (Hz)	Damping factor	In-plane root slope
Out of plane 1	2.201	2.014	0.0050	0.0000
Out of plane 2	2.201	2.014	0.0050	0.0000
Out of plane 3	5.965	5.763	0.0050	0.0000
Out of plane 4	5.965	5.763	0.0050	0.0000
In plane 1	4.262	4.182	0.0050	0.0000
In plane 2	9.241	9.154	0.0050	0.0345
In plane 3	14.397	14.321	0.0050	0.0000
In plane 4	20.526	20.456	0.0050	0.0384

Tower modes

Mode	Frequency (Hz)	Damping factor	Tower top slope
Fore-aft 1	0.874	0.0050	0.0552
Fore-aft 2	6.634	0.0050	-0.7237
Side-side 1	0.886	0.0050	0.0546
Side-side 2	8.712	0.0050	-1.4140

REPORT DOCUMENTATION PAGE

Form Approved
OMB No. 0704-0188

PLEASE DO NOT RETURN YOUR FORM TO THE ABOVE ORGANIZATION.

1. REPORT DATE *(DD-MM-YYYY)*	2. REPORT TYPE	3. DATES COVERED *(From - To)*
December 2010	Technical Report	

4. TITLE AND SUBTITLE
Controller Field Tests on the NREL CART2 Turbine

5a. CONTRACT NUMBER
DE-AC36-08-GO28308

5b. GRANT NUMBER

5c. PROGRAM ELEMENT NUMBER

6. AUTHOR(S)
E. Bossanyi, A. Wright, and P. Fleming

5d. PROJECT NUMBER
NREL/TP-5000-49085

5e. TASK NUMBER
WE10.3131

5f. WORK UNIT NUMBER

7. PERFORMING ORGANIZATION NAME(S) AND ADDRESS(ES)
National Renewable Energy Laboratory
1617 Cole Blvd.
Golden, CO 80401-3393

8. PERFORMING ORGANIZATION REPORT NUMBER
NREL/TP-5000-49085

9. SPONSORING/MONITORING AGENCY NAME(S) AND ADDRESS(ES)

10. SPONSOR/MONITOR'S ACRONYM(S)
NREL

11. SPONSORING/MONITORING AGENCY REPORT NUMBER

12. DISTRIBUTION AVAILABILITY STATEMENT
National Technical Information Service
U.S. Department of Commerce
5285 Port Royal Road
Springfield, VA 22161

13. SUPPLEMENTARY NOTES

14. ABSTRACT *(Maximum 200 Words)*

This document presents the results of the field tests carried out on the CART2 turbine at NREL to validate control algorithms for individual pitch control and active tower damping designed for this turbine by Garrad Hassan & Partners Ltd as part of the European research project 'UPWIND'.

15. SUBJECT TERMS
wind turbine; field tests; CART2; control algorithms; pitch control; active tower damping

16. SECURITY CLASSIFICATION OF:			17. LIMITATION OF ABSTRACT	18. NUMBER OF PAGES	19a. NAME OF RESPONSIBLE PERSON
a. REPORT	b. ABSTRACT	c. THIS PAGE			19b. TELEPHONE NUMBER (*Include area code*)
Unclassified	Unclassified	Unclassified	UL		

Standard Form 298 (Rev. 8/98)
Prescribed by ANSI Std. Z39.18